CCM1–ICAP-1 complex controls β1 integrin–dependent endothelial contractility and fibronectin remodeling

Eva Faurobert,[1,2,3] Claire Rome,[1,3] Justyna Lisowska,[1,2,3] Sandra Manet-Dupé,[1,2,3] Gwénola Boulday,[4] Marilyne Malbouyres,[7] Martial Balland,[3,8] Anne-Pascale Bouin,[1,2,3] Michelle Kéramidas,[1,3] Daniel Bouvard,[1,2,3] Jean-Luc Coll,[1,3] Florence Ruggiero,[7] Elisabeth Tournier-Lasserve,[4,5,6] and Corinne Albiges-Rizo[1,2,3]

[1]INSERM U823, Institut Albert Bonniot, Grenoble F-38042, France
[2]ERL Centre National de la Recherche Scientifique (CNRS) 5284, Grenoble F-38042, France
[3]Université Joseph Fourier, Grenoble F-38042, France
[4]INSERM, UMR-S 740, Université Paris Diderot, Paris F-75010, France
[5]Université Paris 7-Denis Diderot, Faculté de Médecine, Site Lariboisière, Paris, F-75010, France
[6]AP-HP, Groupe hospitalier Saint-Louis Lariboisiere-Fernand-Widal, Paris F-75010, France
[7]UMR CNRS 5242 - ENS Lyon, Lyon F-69634, France
[8]Laboratoire interdisciplinaire de Physique UMR CNRS 5588, Saint Martin d'Hères F-38041, France

The endothelial CCM complex regulates blood vessel stability and permeability. Loss-of-function mutations in CCM genes are responsible for human cerebral cavernous malformations (CCMs), which are characterized by clusters of hemorrhagic dilated capillaries composed of endothelium lacking mural cells and altered sub-endothelial extracellular matrix (ECM). Association of the CCM1/2 complex with ICAP-1, an inhibitor of β1 integrin, prompted us to investigate whether the CCM complex interferes with integrin signaling. We demonstrate that CCM1/2 loss resulted in ICAP-1 destabilization, which increased β1 integrin activation and led to increased RhoA-dependent contractility. The resulting abnormal distribution of forces led to aberrant ECM remodeling around lesions of CCM1- and CCM2-deficient mice. ICAP-1–deficient vessels displayed similar defects. We demonstrate that a positive feedback loop between the aberrant ECM and internal cellular tension led to decreased endothelial barrier function. Our data support that up-regulation of β1 integrin activation participates in the progression of CCM lesions by destabilizing intercellular junctions through increased cell contractility and aberrant ECM remodeling.

Introduction

Familial cerebral cavernous malformations (CCMs) in humans result from mutations of CCM1 (Krit1), CCM2 (malcavernin, OSM, MGC4607), or CCM3 (PDCD10; Riant et al., 2010). CCMs consist of clusters of dilated small vessels embedded in a collagenous matrix whose blood barrier is compromised by gaps between endothelial cells and by the paucity of surrounding mural cells (Wong et al., 2000; Clatterbuck et al., 2001). These lesions affect 0.5% of the worldwide population. They are found in several vascular beds, but the clinical manifestations are deleterious in brain, where the consequence can be hemorrhagic stroke, seizure, or neurological disorders (Chan et al., 2010;

Yadla et al., 2010). Proteomic and cellular analyses have shown that CCM1 and CCM2 proteins associate in a complex recruited at the plasma membrane that directs the formation of adherens and tight junctions (Zawistowski et al., 2005; Glading et al., 2007; Hilder et al., 2007; Faurobert and Albiges-Rizo, 2010) and the localization of the Par polarity complex to these junctions (Lampugnani et al., 2010). CCM1 is an effector of the small G-protein Rap1 known as the master regulator of cell–cell and cell–ECM adhesion (Béraud-Dufour et al., 2007; Glading et al., 2007; Boettner and Van Aelst, 2009). CCM1 and CCM2 regulate actomyosin cytoskeleton contractility through the control

The Rockefeller University Press $30.00
J. Cell Biol. Vol. 202 No. 3   545–561
www.jcb.org/cgi/doi/10.1083/jcb.201303044

JCB   **545**

of RhoA activation and subsequent ROCK activity (Borikova et al., 2010; Chan et al., 2010; Stockton et al., 2010).

Until now, studies on CCM proteins have focused on the regulation of cell–cell junctions. The dialogue of the endothelial cell with its extracellular matrix (ECM) may also be controlled by CCM proteins: there are defects in the ultrastructure of the basal lamina juxtaposed to endothelial cells in human or mouse CCM lesions (Wong et al., 2000; Clatterbuck et al., 2001; Chan et al., 2011; McDonald et al., 2011) and ICAP-1, a negative regulator of β1 integrin, associates with the CCM1–CCM2 complex (Hilder et al., 2007) through direct interaction with CCM1 (Zhang et al., 2001; Zawistowski et al., 2002). ICAP-1 inhibits β1 integrin interaction with ECM (Bouvard et al., 2007; Millon-Frémillon et al., 2008) by binding specifically to β1 integrin cytoplasmic tail (Chang et al., 1997; Zhang and Hemler, 1999; Bouvard et al., 2003, 2006). Integrins are αβ heterodimeric transmembrane receptors that upon activation link the ECM to intracellular signaling pathways and to the actin cytoskeleton, allowing outside-in and inside-out flows of information (Hynes, 2002). Integrins play an important role in tissue morphogenesis by regulating cell adhesion to ECM, cell shape and polarity, cell migration, and actomyosin cytoskeleton architecture as well as ECM deposition and remodeling (Huttenlocher et al., 1996; Papusheva and Heisenberg, 2010; Schwarzbauer and DeSimone, 2011). ICAP-1 is involved in the bidirectional cross talk between the cell and its ECM. It enables the cell to sense and adapt its adhesive and migratory responses to the ECM density (Millon-Frémillon et al., 2008), and regulates ECM organization in bones by controlling fibronectin (FN) fibrillogenesis (Brunner et al., 2011).

FN fibrils are deposited on the cell surface in an α5β1 integrin–dependent process (Singh et al., 2010). FN is a major component of the provisional ECM produced during sprouting angiogenesis. β1 integrin and FN fibrillogenesis are crucial for endothelial tubulogenesis and branching, mural cell apposition, and regulation of lumen diameter (Abraham et al., 2008; Zhou et al., 2008; Stratman et al., 2009; Zovein et al., 2010; Mettouchi, 2012). ICAP-1 stimulates Notch signaling and is anti-angiogenic in HUVECs implanted in mice (Brütsch et al., 2010), but its role on in vivo blood vessel morphogenesis and vascular integrity is unknown.

We show that ICAP-1 is strongly destabilized when either CCM1 or CCM2 is lost, suggesting ICAP-1–associated functions are impaired in human CCM pathology. We demonstrate for the first time that increased cell contractility upon CCM1/2 loss results from higher β1 integrin activation subsequently to ICAP-1 destabilization. As a result of increased β1 integrin activation and redistribution of traction forces to the cell body, CCM1- or CCM2-depleted endothelial cells do not remodel FN correctly. Consistent with our in vitro findings, altered FN remodeling and ECM organization are observed around CCM lesions of CCM1- and CCM2-deficient mice and ICAP-1–deficient blood vessels. Importantly, we demonstrate that a feedback loop between this aberrant ECM and internal tension decreases endothelial barrier function. Altogether, our results support the idea that ICAP-1 loss and β1 integrin activation participate in the progression of CCM lesions by increasing intracellular tensions.

Results

ICAP-1 is stabilized by CCM1 and CCM2

Mouse-inducible endothelial-specific knock-out of CCM1 and CCM2 generates lesions identical to human CCM lesions (Boulday et al., 2011; Chan et al., 2011; Cunningham et al., 2011). Because ICAP-1, a β1 integrin–negative regulator, associates with the CCM1–CCM2 complex through its direct binding to CCM1, we asked whether the stability of ICAP-1 would be affected by the absence of CCM1 or CCM2. CCM1 and CCM2 knock-down in HUVECs led to a dramatic loss of ICAP-1 protein (Fig. 1 A). Less than 10% of ICAP-1 was left in these cells compared with HUVECs transfected with CT siRNA (Fig. 1 B). A similar loss of ICAP-1 was observed in $ccm2-/-$ embryos (Fig. 1 D and Fig. S1 A), confirming our results in vivo. CCM1 level was also strongly reduced in ICAP-1– or CCM2-silenced HUVECs (Fig. 1, A and B) and in tissues from CCM2- or ICAP-1–invalidated mice (Fig. 1, D and E; and Fig. S1 B). CCM2 was much less affected by the loss of its CCM partners; ∼70% of CCM2 remained upon ICAP-1 and CCM1 loss (Fig. 1, A and B). ICAP-1 and CCM1 losses were not due to reduced gene expression (Fig. 1 C), but instead to protein instability. Overexpression of CCM1 together with ICAP-1 inhibited the proteasomal degradation of ICAP-1 and prolonged its lifetime in CHO cells after blockage of protein synthesis by cycloheximide (Fig. 1, F and G). CCM1–ICAP-1 interaction was necessary for ICAP-1 stabilization: A mutant of CCM1 unable to interact with ICAP-1 (CCM1 N192A-Y195A; Zhang et al., 2001) did not stabilize ICAP-1 (Fig. 1, F and G), and the fusion to ICAP-1 of the N terminus of CCM1 containing ICAP-1–binding site strongly improved the solubility of ICAP-1 produced in bacteria (unpublished data). Overexpression of CCM2 together with ICAP-1 did not significantly prolong ICAP-1 lifetime, consistent with the absence of a direct interaction between the two proteins (Fig. 1 G). However, coexpression of CCM2 together with CCM1 significantly increased ICAP-1 lifetime compared with coexpression of CCM1 alone (Fig. 1 G). This suggests that CCM2 stabilizes CCM1, which in turn stabilizes ICAP-1 by interacting with it. We were not able to measure CCM1 and CCM2 lifetimes, probably because they are much longer than that of ICAP-1 and not measurable because of the toxicity of cycloheximide when added for too long on the cells. Overall, our studies strongly support that ICAP-1 and CCM1 are mutually stabilized by their interaction and that CCM2 acts as a scaffold for this binary complex. Importantly, the ICAP-1–CCM1 complex is lost upon in vivo or in vitro depletion in CCM1 or CCM2.

CCM1 and CCM2 control β1 integrin activation and spatial distribution

ICAP-1 inhibits the activated state of β1 integrin and controls the distribution of β1 integrin–containing focal adhesions (Bouvard et al., 2007; Millon-Frémillon et al., 2008). Because CCM1- or CCM2-depleted HUVECs express much less ICAP-1 protein than CT cells, we asked whether CCM1/2 loss would impact β1 integrin activation. We examined activated β1 integrin state by flow cytometry using an activated state-specific antibody, 9EG7 (Bazzoni et al., 1995). Flow cytofluorometry was performed
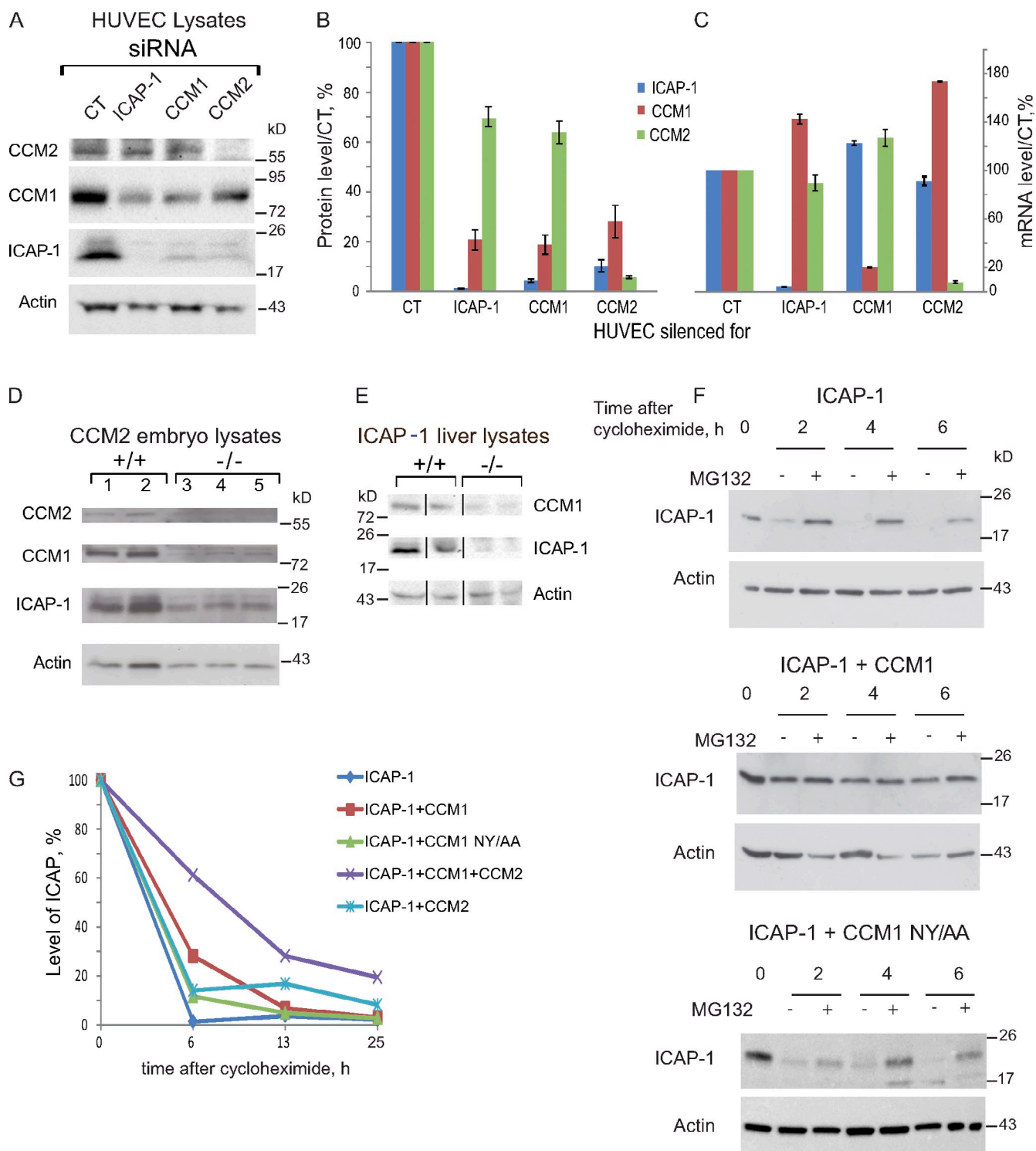
Figure 1. **CCM1 and ICAP-1 proteins are destabilized upon CCM1 and CCM2 loss.** (A) ICAP-1, CCM1, and CCM2 protein content in total lysates of KD HUVECs was analyzed by Western blot. (B) Quantification of the three proteins normalized to actin in silenced HUVEC; Error bars are ± SEM (*n* = 3). ICAP-1 and CCM1 proteins were strongly reduced in the three conditions. (C) Q-PCR measurements show that knock-down of one protein had not effect on the expression of the two other partners. Error bars are means ± SEM (*n* = 3). (D) Western blot of CCM2 +/+ and −/− embryo lysates showing the loss of CCM1 and ICAP-1 proteins upon CCM2 depletion. Remaining CCM2 comes from maternal material. (E) Western blot of ICAP-1 andCCM1 in liver lysates from ICAP-1+/+ and ICAP-1−/− mice. One fourth of CCM1 protein remains in ICAP-1−/− mice (see Fig. S1 C for densitometric analysis). Black lines indicate that intervening lanes have been spliced out for presentation purposes. (F) Overexpressed ICAP-1 protein in CHO is stabilized by the coexpression of CCM1 but not of the N192-Y195 non-interacting CCM1 mutant. Cycloheximide was added at t = 0 to block protein synthesis with or without the proteasomal inhibitor MG132. Results are representative of three independent experiments. (G) Quantification of ICAP-1 protein level over a time-course after addition of cycloheximide when expressed alone or in different combinations with CCM1 and/or CCM2. Results are representative of two independent experiments.

under blebbistatin treatment to relax the actomyosin cytoskeleton and eliminate any contribution of cortical cytoskeleton tension to β1 integrin activation. CCM1- and CCM2-silenced HUVECs displayed a higher percentage of activated β1 integrin than CT cells on their cell surface similarly to ICAP-1–silenced HUVECs, consistently with their loss in ICAP-1 (Fig. 2 A).

When sparsely adhered onto FN, these CCM1-, CCM2-, and ICAP-1–silenced cells formed more β1 integrin–containing adhesions on their ventral surface. Whereas CT HUVECs displayed limited peripheral staining for activated β1 integrin, three times more CCM1- or CCM2-depleted HUVECs contained longer linear tracks of activated β1 integrin all over the ventral side of the cell (Fig. 2, B and C), similarly to ICAP-1–depleted HUVECs. Talin colocalized with β1 integrin in these focal adhesions, consistent with an increase in β1 integrin signaling (Fig. S2). These results establish that CCM proteins regulate β1 integrin activation and spatial distribution on the cell surface.

CCM1 and CCM2 require β1 integrin to activate RhoA

CCM1 and CCM2 loss results in a higher level of RhoAGTP, which is deleterious for the endothelial permeability barrier (Whitehead et al., 2009; Borikova et al., 2010; Stockton et al., 2010). β1 integrin–dependent cell adhesion to ECM is known as a signal for RhoA activation and cell contractility (Huveneers and Danen, 2009). We wondered whether increased RhoA activation could be mediated by increased β1 integrin signaling upon CCM loss. We therefore performed RhoAGTP pull-down assays in conditions where ICAP-1– and CCM1/2-silenced HUVECs were additionally silenced for β1 integrin. We confirmed that loss of CCM1 and CCM2 led to increased RhoAGTP (Fig. 2 D). In addition, ICAP-1 loss also increased RhoA activation by a similar fold (Fig. 2 D) Supplemental silencing of β1 integrin (Fig. S3 A) completely abolished this increase of RhoAGTP (Fig. 2 E), which remained at the level of CT cells (Fig. S3 B). Our results show the crucial role of β1 integrin in RhoA activation upon ICAP-1 and CCM protein loss.

CCM1 and CCM2 control the architecture of β1 integrin–dependent actin cytoskeleton and the distribution of cellular traction forces

Adhesion of cells to ECM allows the generation of traction forces by the contractile actomyosin cytoskeleton (Huveneers and Danen, 2009; Parsons et al., 2010). Actomyosin contractility is up-regulated in CCM-depleted cells as a result of increased RhoA activation and ROCK-dependent myosin phosphorylation (Whitehead et al., 2009; Borikova et al., 2010; Stockton et al., 2010). Sparse HUVECs depleted in CCM1, CCM2, or ICAP-1 were more elongated than CT HUVECs and displayed transversal bundles of actin fibers connected to β1 integrin–containing focal adhesions (Fig. 2, F and H). Additional depletion in β1 integrin blocked the formation of these actin bundles and rescued the wild-type cell shape and cortical actin cytoskeleton (Fig. 2, F and H). This effect was specific for β1 integrin depletion; additional β3 integrin knock-down had no effect (Fig. 2, F and H). β1 integrin depletion alone did not strongly modify the architecture

of the actin cytoskeleton (Fig. 2 F), suggesting that in normal endothelial cells, CCM1/2 proteins maintain the activity of β1 integrin low and thereby limit its effect on the actin cytoskeleton.

On confluent HUVECs, the appearance of transversal stress fibers upon CCM1 or 2 loss is associated with reduced VE-cadherin and β catenin staining to cell–cell junctions (Glading et al., 2007; Whitehead et al., 2009).Similarly, ICAP-1 silencing led to an increase in actin stress fibers on confluent HUVECs and to a decrease in VE-cadherin and β-catenin junctional staining (Fig. 2 G, Fig. S4). Additional depletion in β1 integrin but not in β3 integrin led to the disappearance in the transversal actin fibers on confluent monolayers of HUVECs (Fig. 2 G), showing that in confluent as in sparse HUVECs, the control of the actin cytoskeleton architecture by CCM proteins involves β1 integrin.

Because CCM1 or CCM2 loss in HUVECs changed the architecture of the actin cytoskeleton, we hypothesized that the distribution of the traction forces developed by these cells would be modified. Phosphorylated myosin light chain (pMLC) and zyxin, which localize to tense actomyosin fibers (Colombelli et al., 2009), were uniformly distributed along the transversal actin fibers in CCM1-, CCM2-, or ICAP-1–depleted HUVECs, as compared with their peripheral localization in CT cells (Fig. 3 A). Additional silencing of β1 integrin in sparse ICAP-1– or CCM1/2-silenced HUVECs restored the peripheral localization of pMLC and zyxin, whereas β3 integrin depletion did not (Fig. S3 D). To correlate the relocalization of these tension markers with the forces developed by these cells, we visualized by traction force microscopy the distribution of the forces when cells were plated on FN-coated polyacrylamide gels. Forces were concentrated in the cell periphery in CT HUVECs (Fig. 3, B and C), which is consistent with a peripheral localization of focal adhesions and actin cytoskeleton. However, in CCM1-, CCM2-, and ICAP-1–depleted cells, the traction forces redistributed to central patches, consistent with the relocalization of pMLC and zyxin. Therefore, CCM proteins regulate the shape of endothelial cells, the architecture of their actomyosin cytoskeleton, and the distribution of their traction forces by controlling β1 integrin activity.

CCM1 and CCM2 control β1 integrin–dependent FN remodeling

Upon ROCK-dependent traction by the actomyosin cytoskeleton, α5β1 FN-engaged integrins translocate toward the cell body, allowing unfolding of FN cryptic sites and FN polymerization in fibers (Clark et al., 2005). Having shown that activated β1 integrin and cell tension are redistributed over the cell surface upon loss of CCM1 or CCM2, we analyzed the capacity of HUVECs to remodel glass-coated FN in vitro. After 24 h, CT HUVECs had woven a network of FN fibers with a hairy appearance (Fig. 3 D), whereas CCM1- or CCM2-silenced HUVECs silenced similarly to ICAP-1–depleted cells generated more but shorter streaks of FN all over the cell ventral face underneath the numerous β1 integrin focal adhesions. These streaks had grown following the direction of the actin stress fibers, resulting in a linear array of parallel and short lines of FN (Fig. 3 D). On a confluent monolayer after 48 h of culture, these defects led to a network of straight and parallel FN fibers, whereas CT HUVECs generated a mesh-patterned network of interlaced FN
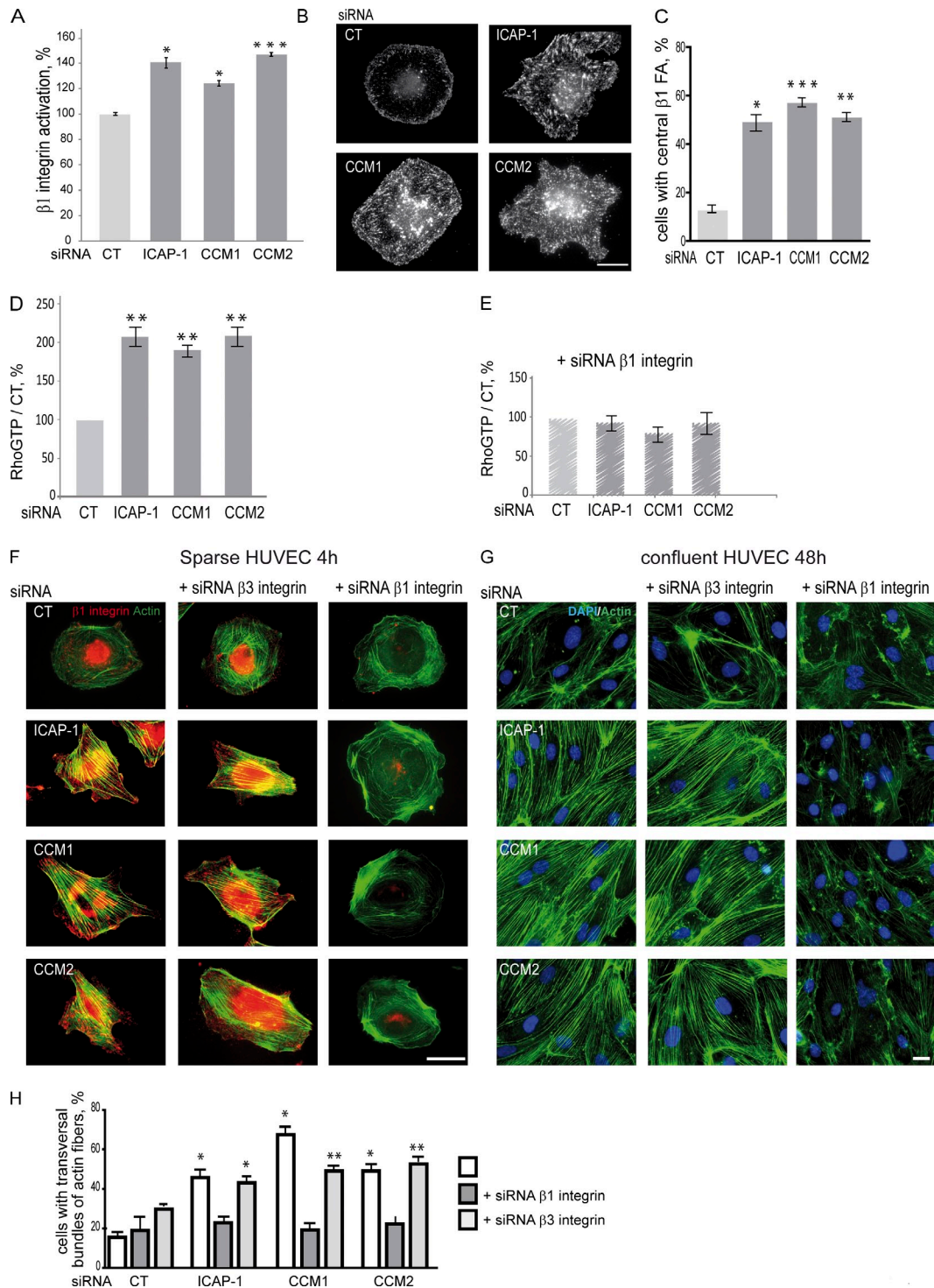
Figure 2. **CCM1/2 proteins control RhoA-dependent actin cytoskeleton organization by regulating β1 integrin activation.** (A) Flow cytofluorometry using 9EG7 shows an increase in β1 integrin activation upon silencing of CCM1, CCM2, or ICAP-1. Error bars are means ± SEM ($n = 4$). (B) HUVECs depleted in ICAP-1, CCM1, or CCM2 spread for 1 h on low density of FN displayed more and larger β1 integrin containing focal adhesions (stained with 9EG7 antibody) localized all over their ventral face. Bar, 5 μm. (C) Quantification of the percentage of cells displaying central plaques. Error bars are means ± SEM ($n = 3$). (D and E) Quantification of RhoA activation upon ICAP-1, CCM1, or CCM2 depletion alone (D) or with additional β1 integrin silencing (E) by RhoGTP pull-downs. Error bars are means ± SEM ($n = 3$). RhoG-LISA measurements show that the level of RhoAGTP returned to that of CT upon ICAP-1 or CCM1/2 depletion in absence of β1 integrin (see Fig. S3 B). (F) Transversal actin bundles were observed in elongated HUVECs upon depletion of ICAP-1, CCM1, or CCM2 spread on FN for 4 h. Additional siRNA depletion of β1 but not of β3 integrin (Fig. S3 A) abolished their formation. (G) As sparse cells, confluent HUVECs displayed transversal actin stress fibers and their junctional VE-cadherin and β-catenin stainings appeared thinner and discontinuous (see Fig. S4). Transversal actin fibers were abolished upon additional depletion in β1 but not in β3 integrin. (H) Quantification of the percentage of sparse cells with transversal actin bundles in the absence or presence of additional β1 or β3 integrin depletion. Error bars are means ± SEM ($n = 3$). *, $P < 0.05$; **, $P < 0.005$; ***, $P < 0.0005$.
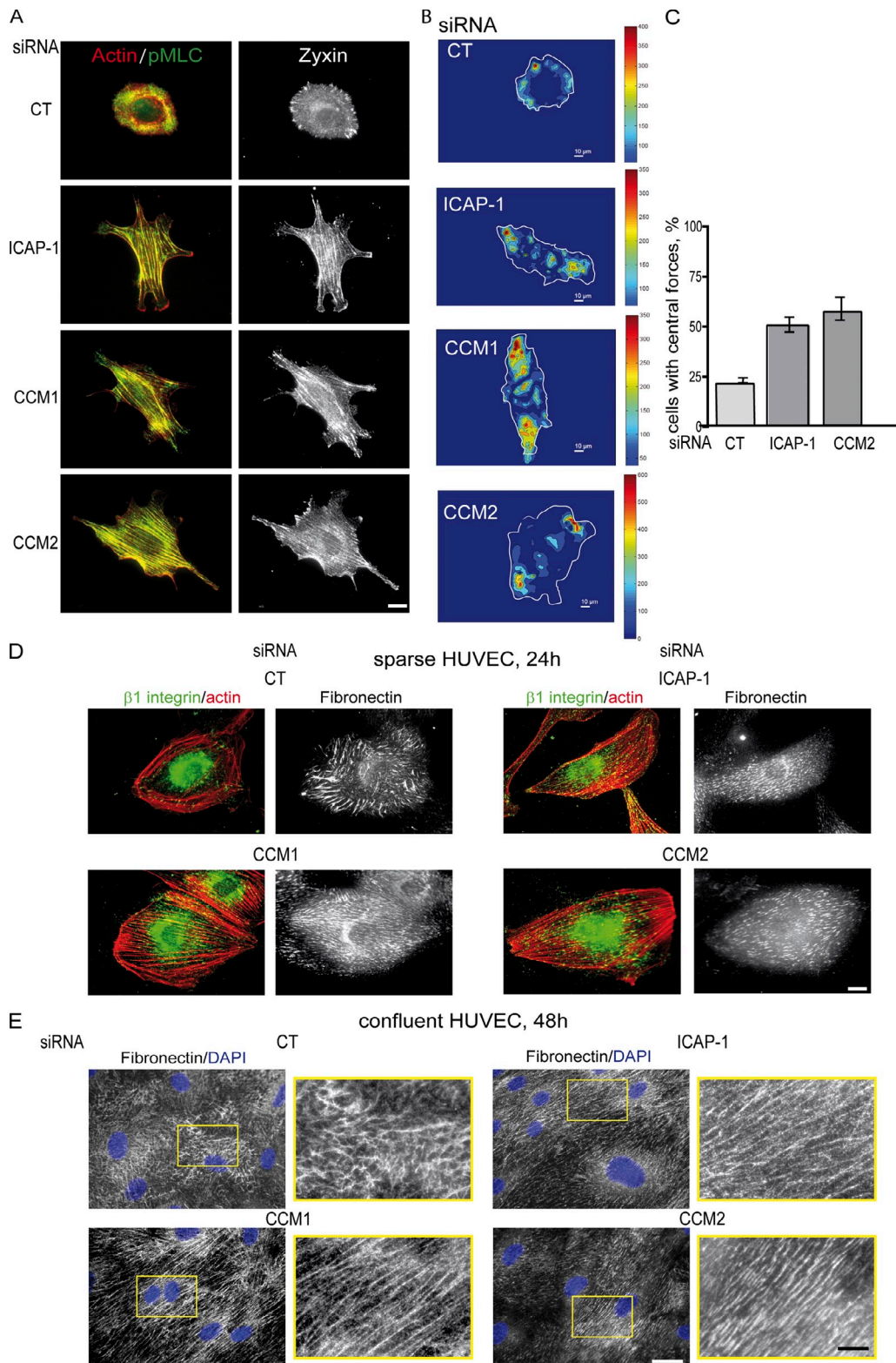
Figure 3. **CCM1/2 proteins control β1 integrin–dependent distribution of traction forces and FN remodeling.** (A) pMLC and zyxin delocalized from the peripheral focal adhesions to transversal actin stress fibers upon depletion in ICAP-1, CCM1, or CCM2 after 4 h of spreading. Bar, 5 μm. These images are presented again in Fig. S3 C, where it is shown that pMLC and zyxin relocalized to the cell periphery upon additional silencing of β1 integrin but not of β3 integrin. (B) Representative traction forces maps obtained by TFM. Forces were delocalized from the cell periphery to all over the ventral face upon CCM depletion. (C) Quantification of the percentage of cells displaying central traction forces. Between 14 and 23 cells of each were analyzed. Error bars are means ± SEM (n = 2). Similar fold-increase of the percentage of cells bearing central forces was measured for CCM1-depleted HUVECs (n = 1; not depicted). Bar, 10 μm. Remodeling of glass-coated FN was studied on sparse cells after 24 h (D) and on confluent cells after 48 h (E). Bars, 5 μm. FN staining in the yellow box in E is magnified to highlight the linear pattern of parallel FN fibers produced by ICAP-1/CCM-depleted HUVECs. Bars, 2 μm. These data are representative of more than three independent experiments.
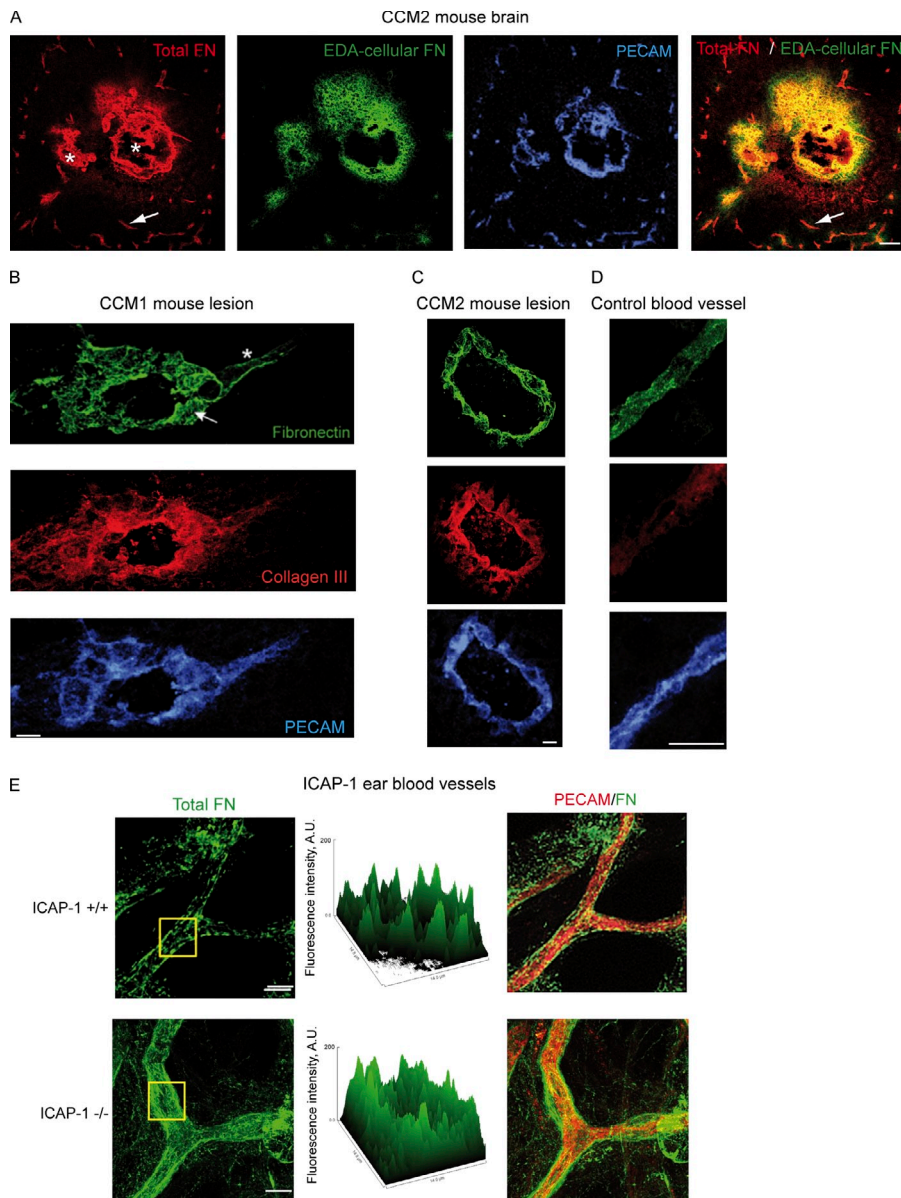
A CCM2 mouse brain

Total FN | EDA-cellular FN | PECAM | Total FN / EDA-cellular FN

B CCM1 mouse lesion

Fibronectin
Collagen III
PECAM

C CCM2 mouse lesion

D Control blood vessel

E ICAP-1 ear blood vessels

Total FN | PECAM/FN

ICAP-1 +/+

ICAP-1 -/-

Figure 4. **Abnormal FN deposition around mouse CCM1 or CCM2 lesions and ICAP-1–deficient blood vessels.** (A) Sections of iCCM2 were labeled with total FN, cFN, and PECAM. CCM lesions are annotated by asterisks and normal blood vessels by arrows. cFN was abundant around CCM lesions, but barely detectable around peri-lesion blood vessels. Bar, 50 µm. (B and C) Numerous FN fibers appeared around the lesions (B, arrow), whereas FN signal was weak and diffuse around unaffected peri-lesion vessels (B, asterisk) or CT blood vessels (D). Strong collagen III staining was detected around CCM lesions but not around unaffected peri-lesion vessels or CT blood vessels. $n = 3$ mice for iCCM1, $n = 6$ mice for iCCM2. Bars, 10 µm. (E) Projections of confocal z-stacks of whole-mount of ear blood vessels of ICAP-1 +/+ and −/− mice immunostained for PECAM and FN. Blood had been washed out by intracardiac perfusion of PBS. The plot of intensity of the FN signal over the surface delineated by the yellow square is presented in the middle. Increased FN deposition as a mixture of soluble and thin fibrils around ICAP-1−/− blood vessels differed from the discrete FN fibers around ICAP-1+/+ blood vessels. $n = 3$ from two litters for each genotype. Bars, 10 µm.

fibers (Fig. 3 E). Additional silencing of β1 integrin in endothelial cells depleted in ICAP-1 or CCM1/2 and inhibition of ROCK using Y27632 totally suppressed FN fibrillogenesis (unpublished data), confirming that the defect in fibrillogenesis depended on the activity of β1 integrin and ROCK. Therefore, we showed that by controlling the architecture of β1 integrin–dependent adhesions and cell traction forces, CCM proteins function as regulators of FN assembly in vitro.

Human and mouse CCM lesions show foci of multilayered or disrupted basal lamina surrounded by a collagenous interstitial matrix (Wong et al., 2000; Clatterbuck et al., 2001; Chan et al., 2011; McDonald et al., 2011). Because FN fibrillogenesis is required for ECM assembly (Schwarzbauer and DeSimone, 2011), we asked whether FN deposition and remodeling would be affected in CCM lesions, as for in vitro cultures. For this, endothelial-specific knock-out of CCM1 and CCM2 was induced in mice by tamoxifen (iCCM1 and iCCM2; Boulday et al., 2011). Brain sections were labeled with antibodies against PECAM to label

endothelial cells, extra domain A–containing cellular FN (cFN), total FN, and with collagen III. The first striking result was the presence around CCM lesions of large amounts of EDA cFN, a marker of angiogenic vessels, which had invaded the neuronal tissue, whereas barely detectable around normal blood vessels (Fig. 4 A). A profusion of FN fibrils were wrapped around the CCM1 lesion, whereas a uniform and weak FN signal was detected around the adjacent unaffected part of the blood vessel (Fig. 4 B) or around blood vessels of CT animals (Fig. 4 D). Similar numerous FN fibrils were present around CCM2 lesions (Fig. 4 C). FN fibrillogenesis is a critical regulator of collagen deposition (Velling et al., 2002). Consistently, strong collagen III staining colocalized with FN fibers around CCM lesions (Fig. 4, B and C), whereas staining was barely detectable around blood vessels of CT animals (Fig. 4 D). Thus, aberrant FN deposition and remodeling were associated with the lesions in iCCM1 and iCCM2 models.

FN deposition was then analyzed around ICAP-1–deficient blood vessels. After staining of whole-mount ear outer leaflet
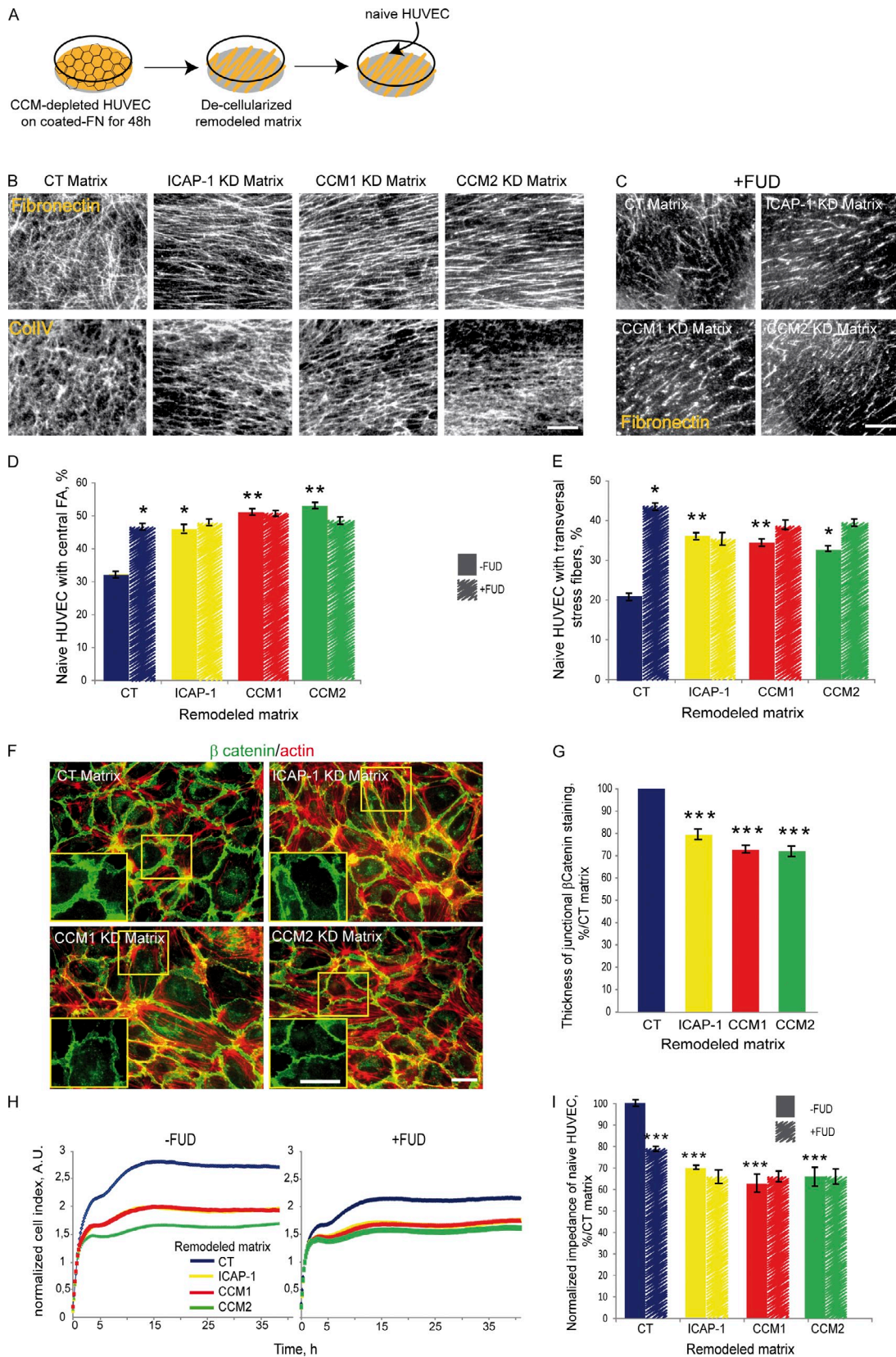
Figure 5. **Defective ECM organization increases cellular tension and decreases barrier function of naive HUVECs.** (A) ICAP-1-, CCM1-, or CCM2-depleted HUVECs were seeded at confluency on FN-coated slides. Cells were removed 48 h later by a triton/ammonium hydroxide treatment. Naive HUVECs were seeded on these decellularized remodeled matrices. (B and C) FN and CollV staining of decellularized matrices remodeled in the absence (B) or presence of FUD (C). Note the linearity of FN fibers and CollV in ICAP-1- and CCM1/2-depleted conditions. Bars, 1 µm. (D) Quantification of the percentage of naive HUVECs with central β1 integrin focal adhesions after 1 h of spreading. (E) Quantification of the percentage of naive HUVECs with transversal stress fibers

with PECAM and FN antibodies, a well-organized network of discrete FN fibrils was detected around the blood vasculature of *icap-1+/+* mice, as shown on projections of confocal z-stack images (Fig. 4 E). Surface plot analysis of the FN staining in the square highlights the distribution of well-separated peaks of fluorescence corresponding to discrete FN fibrils. FN was differently deposited around *icap-1−/−* blood vessels (Fig. 4 E). The overall intensity of the labeling was higher than that of *icap-1+/+* blood vessels, corresponding to an increased secretion of FN around ICAP-1–deficient blood vessels, as observed around CCM lesions. The FN labeling consisted of more numerous FN fibrils over a higher background of soluble FN than in CT vessels. Therefore, our in vitro and in vivo results show that CCM1 and CCM2, most likely through ICAP-1 regulation, control β1 integrin–dependent FN remodeling.

ECM organization feeds back onto endothelial cell tension and barrier function

To ensure homeostasis, cells adapt their contractile behavior to external tension. We asked whether aberrant FN fibrillogenesis by CCM-depleted endothelial cells could favor the development of CCM lesions as already described in cancer or vascular diseases (Larsen et al., 2006). For this, remodeled ECM from CCM-depleted HUVECs was presented to naive HUVECs to test its capacity to modify their contractile behavior and junctional functionality. CCM1/2- and ICAP-1–silenced HUVECs were cultured for 48 h on FN-coated plates to allow FN remodeling. The cells were removed by a triton/ammonium hydroxide treatment, and naive HUVECs were seeded on the resulting decellularized ECM, which were called CCM KD matrices (Fig. 5 A). As shown in Fig. 3, FN matrices generated by CCM- or ICAP-1–depleted HUVECs were made of parallel and linear fibers compared with the network of woven fibers in the CT matrix (Fig. 5 B). FN is a scaffold for many proteins of the ECM (Sottile and Hocking, 2002). As such, collagen IV deposition followed that of FN (Fig. 5 B), demonstrating the more global effect of FN remodeling on the ECM structure. In additional experiments, FN remodeling was inhibited using FUD to study the effect of ECM structure rather than composition through inhibition of its polymerization in fiber (Tomasini-Johansson et al., 2001). At the dose used in these experiments, inhibition was only partial, causing the polymerization of small and linear stiches of FN in all conditions, in CT matrices similarly to CCM or ICAP-1-KD ones (Fig. 5 C).

Strikingly, the percentage of naive HUVECs with central β1 integrin–dependent focal adhesions and pMLC-decorated transversal actin stress fibers increased when they were plated on CCM1/2 or ICAP-1 KD matrices, compared with the CT matrix (Fig. 5, D and E). Using FUD as an ECM disorganizer, FUD treatment of CT matrix increased the percentage of cells with central focal adhesions and transversal stress fibers to a level comparable to CCM–ICAP-1 KD matrices (Fig. 5, D and 5E). Our results

show that the structure of the ECM remodeled by CCM-depleted HUVECs impacts the adhesive and contractile behaviors of naive HUVECs. The array of parallel and straight fibers of FN is sufficient to increase β1 integrin–dependent cell contractility.

To determine whether the feedback loop between remodeled ECM and cell contractility impacts cell–cell junctions, naive HUVECs were seeded at confluency on these matrices and labeled 24 h later for β catenin and actin. As observed at low cell density, CCM–ICAP-1 KD matrices generated a higher percentage of cells with transversal actin stress fibers associated with a thin β catenin staining at cell–cell junctions as compared with CT matrix (Fig. 5 F). Statistical analysis confirmed that β catenin staining was significantly thinner on CCM–ICAP-1 KD matrices (Fig. 5 G). Functionally, the electrical impedance of the monolayer of naive HUVECs was reduced equally for cells plated on the CCM or ICAP-1 KD matrices compared with the CT (Fig. 5, H and I). Therefore, the morphological defects in cell–cell junctions induced by CCM–ICAP-1 KD matrices were associated with a reduced endothelial barrier function. When naive HUVECs were plated on matrices remodeled with FUD, the difference in the electrical resistance between CT and CCM KD matrices was strongly reduced (Fig. 5, H and I), highlighting the crucial effect of the geometry of ECM remodeling in cell permeability. Consistently, the small stiches of FN remodeled by CT HUVECs in presence of FUD gave rise to a defective matrix for cell–cell junctions as CCM KD matrices did.

Altogether, our results show that the organization of FN fibers impacts the endothelial cell contractility and permeability barrier function. These results support the idea that aberrant remodeling of FN around CCM lesions feeds back onto endothelial cells to worsen morphological and functional defects generated by CCM 1 or 2 loss.

ICAP-1–deficient blood vessels display ultrastructural ECM defects and increased permeability

To investigate whether ICAP-1 destabilization upon CCM loss could contribute to the production of an abnormal microenvironment around CCM lesions, we examined *icap-1−/−* blood vessel walls at the ultrastructural level by transmission electron microscopy. Fig. 6, A–C, shows retinal and choroidal vessel ultrastructures. The *icap-1−/−* retinal capillaries were frequently more dilated than the *icap-1+/+* ones (Fig. 6 A), despite pericyte coverage. The dense structure of the basal lamina around capillaries or venules was locally disrupted, appearing lamellated and spotty (Fig. 6 A), torn (Fig. 6 B), or interrupted by large vacuoles (Fig. S5 A). Multilayering of basal lamina directly apposed onto the endothelium was also observed around the fenestrated choroidal *icap-1−/−* capillary (Fig. 6 C) and around a retinal *icap-1−/−* artery (Fig. S5 B). Whereas no structural defect in cell–cell junctions was detected and tight junctions were found

after 4 h of spreading. (F) β-catenin and actin staining of confluent naive HUVECs on the remodeled matrices after 24 h. Bars, 5 µm. (G) Quantification of β-catenin staining thickness showing thinner junctions of CCM KD matrices. (H) Time-course measurement of the electrical impedance of a monolayer of naive HUVECs on these matrices. The data shown are from a single representative experiment out of three repeats. (I) Normalized impedance to that on CT matrix showing a significant decrease of monolayer resistance barrier on CCM KD matrices due to structural changes in FN remodeling. Error bars are ± SEM ($n = 3$). *, $P < 0.05$; **, $P < 0.005$; ***, $P < 0.0005$ using GLMM with Tukey's test.

Figure 6. Ultrastructural defects of the basal lamina and interstitial ECM around ICAP-1–deficient blood vessels are associated with increased permeability to small molecules. (A) Transmission electron micrographs of retinal capillaries showing dilation of ICAP-1−/− capillary compared with ICAP+/+. Bar, 1 µm. Enlargements of the yellow square show that basal lamina (BL) around ICAP-1−/− capillary present zones of multilayering due to dispersion of the dense matter and zones of accumulation of matter in spots (arrows). EC, endothelial cell; P, pericyte. Bar, 0.5 µm. (B) Arrows indicate zones of tearing of the basal lamina around an ICAP-1−/− venule. SMC, smooth muscle cell. Bar, 1 µm. (C) Fenestrated choroidal capillaries showing multilayering of the basal lamina (BL) juxtaposed to EC and enlargement of the interstitial ECM, which appears scattered around ICAP-1−/− capillary. Arrowhead points to detachment of the EC from its BL. EC–EC junctions are present (arrow). Bar, 1 µm. *n* = 4 for each genotype from three litters. (D) Gallery of ear pictures over time under a fluorescence microscope after injection of Alexa Fluor 546/10-kD dextran in the blood circulation. See the progressive increase in fluorescence of the ear tissue in ICAP-1−/− mouse compared with wild-type littermate (yellow rectangle). Bar, 100 µm. (E) Diffusion rate of the 10-kD dextran was calculated between 90 and 300 s after injection. Error bars are means ± SEM (*n* = 5 for each genotype from five litters for +/+ and two litters for −/−). *, $P < 0.05$ one-tailed paired *t* test.
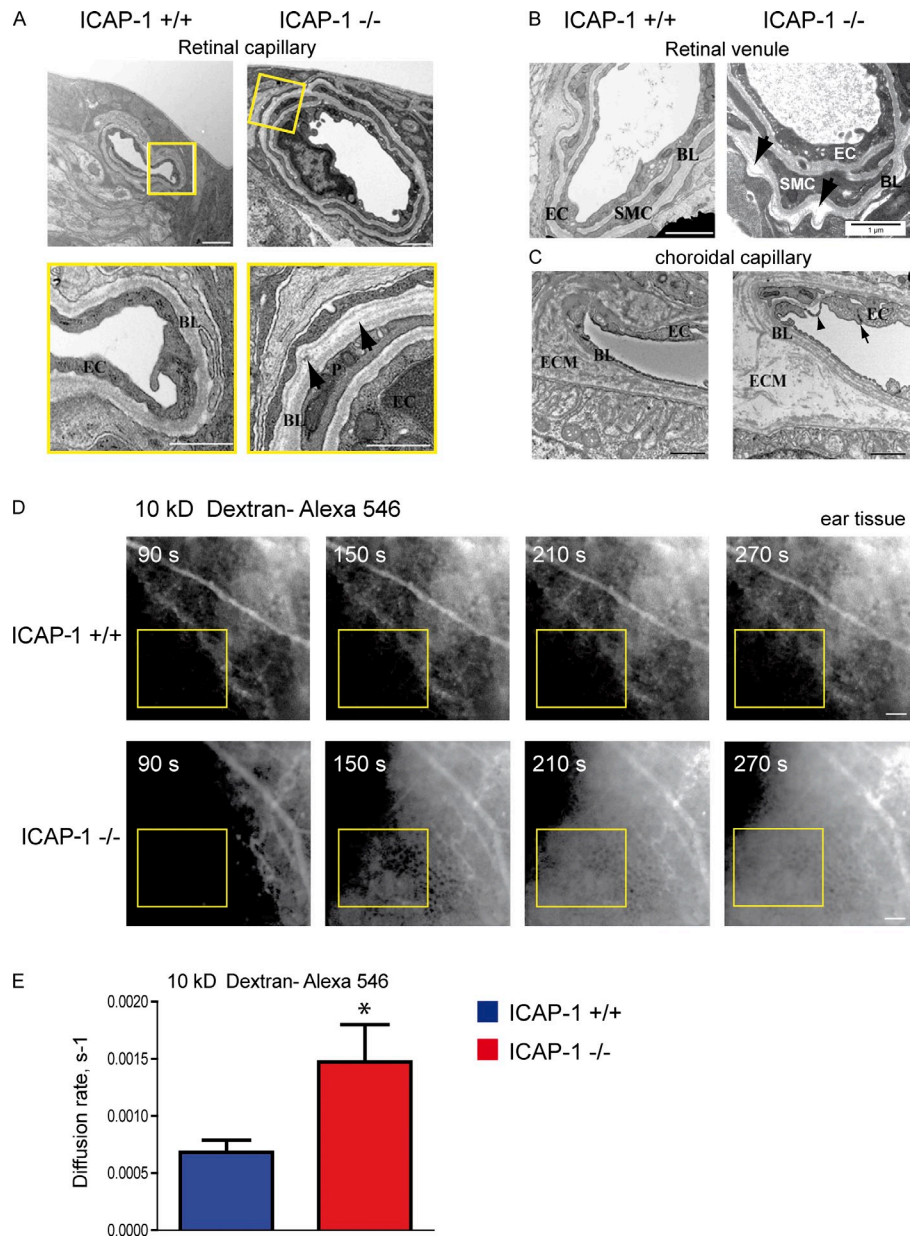
between endothelial cells (Fig. 6 C, arrow), zones of detachment of the endothelial cell from its basal lamina were observed (Fig. 6 C, arrowhead). The interstitial ECM around the *icap-1−/−* choroidal capillary was also abnormally enlarged and less dense in fibers than in the wild-type vessel (Fig. 6 C). These ultrastructural defects are strikingly reminiscent of those around human and mouse CCM lesions (Wong et al., 2000; Clatterbuck et al., 2001; Chan et al., 2011; McDonald et al., 2011), supporting the idea that ICAP-1 loss upon CCM1 or CCM2 depletion could cause the aberrant ECM remodeling around CCM lesions.

As the ECM barrier accounts for 50% of the total barrier function of blood vessels (Mehta and Malik, 2006), we next asked whether these ultrastructural ECM defects of ICAP-1–deficient blood vessels were associated with increased permeability. The permeability of *icap-1−/−* blood vessels was measured by monitoring the extravasation of fluorescent 10- and 70-kD dextran from blood vessels to the ear tissue. The 70-kD dextran diffused

neither from *icap-1−/−* mice blood vessels nor from *icap-1+/+* (Fig. S5 C), but the diffusion of the 10-kD dextran differed significantly between *icap-1−/−* and wild-type blood vessels (Fig. 6 D). Indeed, the diffusion rate in the 5-min after injection was twofold higher for *icap-1−/−* mice than for wild-type littermates (Fig. 6 E), indicating a higher permeability of *icap-1−/−* blood vessels to small molecules. Thus, the ultrastructural defects of the basal lamina of ICAP-1–deficient blood vessels were accompanied by an increased permeability, demonstrating that ICAP-1 has a role in maintaining in vivo barrier function in the endothelium.

ICAP-1 is required for the morphological integrity of blood vessels

To evaluate the contribution of ICAP-1 to blood vessel morphogenesis in vivo, we studied the blood vasculature of ICAP-1 knock-out mice. Contrary to constitutive or endothelial-specific
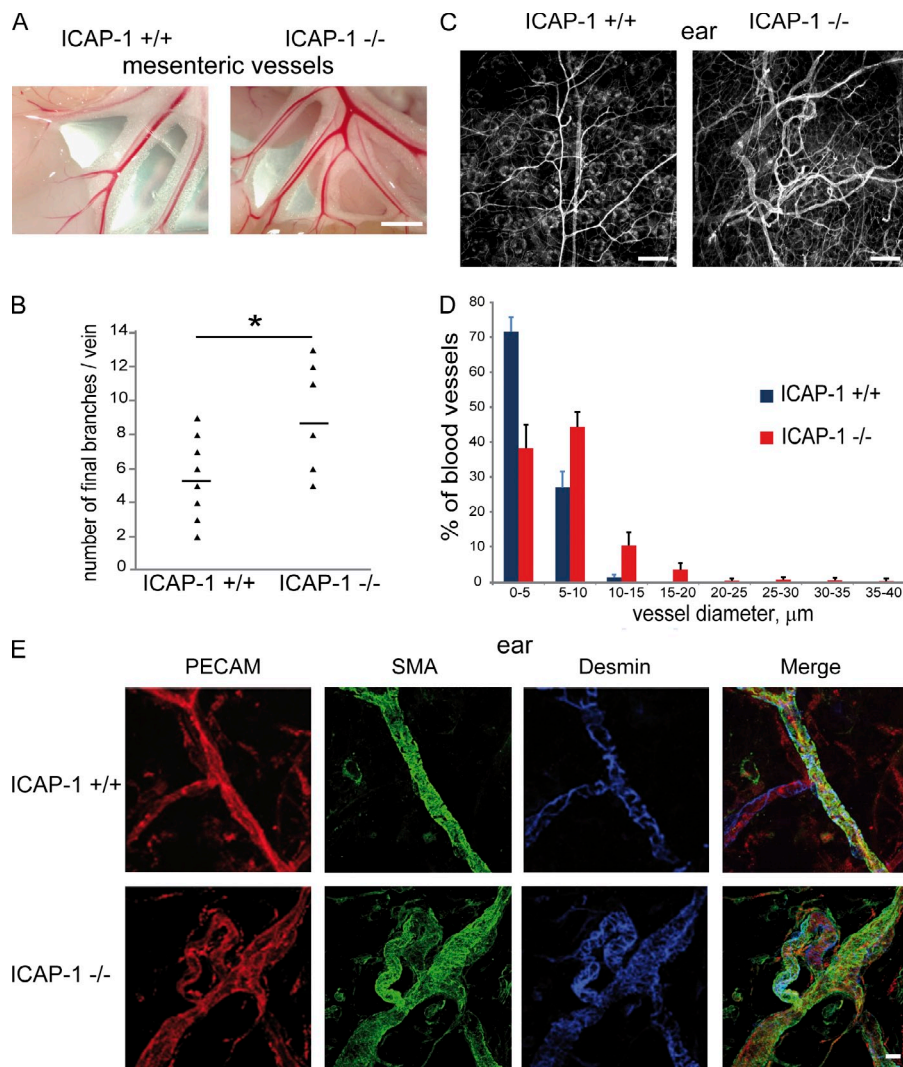
Figure 7. **ICAP-1–deficient mice present dilated, more branched and tortuous blood vessels.** (A) Mesenteric veins of ICAP-1−/− mice were dilated and more branched than in their wild-type littermates. Bar, 5 mm. (B) Quantification of the number of final branches connecting the intestine per mesenteric vein. Points correspond to the number of branches of an individual vein and horizontal bars are the means per genotype (ICAP-1+/+, n = 5 mice from five litters; ICAP-1−/−, n = 4 mice from three litters). *, P < 0.05. (C) Projections of confocal z-stacks of ear whole-mount staining of blood vessels with PECAM. Bar, 100 µm. (D) Histogram of the distribution of blood vessel diameter categories (ICAP-1+/+, n = 4 mice from three litters; ICAP-1−/−, n = 5 mice from two litters). (E) Projections of confocal z-stacks of ear whole-mount staining of blood vessels with PECAM, smooth muscle actin (SMA), and desmin. Bar, 10 µm.

deletion of CCM1 or CCM2 in mice, germline deletion of ICAP-1 does not lead to embryonic lethality, but mice reach adulthood with more or less perinatal mortality depending on their genetic background (Bouvard et al., 2007). Whereas histological analyses of the brains of *icap-1−/−* mice did not reveal CCM lesions (unpublished data), macroscopic observations indicated pleiotropic defects in the topography of the vasculature and in the integrity of the blood vessels of adult ICAP-1–deficient mice. First, dissection of their skin under anesthesia generated massive bleeding. Second, hemorrhages and edemas were frequent on organs like kidneys or ovaries. As such, 8 out of 10 *icap-1−/−* mice had hemorrhagic kidneys (Fig. S5 D), suggesting their blood vessels are fragile. Their vena cava was often dilated (Fig. S5 E). Finally, their mesenteric veins were more branched (Fig. 7, A and B). We then focused on the outer ear tissue to analyze blood vessel morphology. Fig. 7 C shows whole-mount PECAM immunostaining of the outer leaflet of the ear. Blood vasculature of *icap-1−/−* mice presented a chaotic arrangement of dilated and tortuous vessels with undulations, loops, and irregular diameters. Quantification of the diameters revealed a shift of the population of ICAP-1–deficient vessels toward vessels larger than wild-type ones (Fig. 7 D). Confocal image projections at higher

magnifications (Fig. 7 E) confirmed the tortuosity of the ICAP-1–deficient vessels and their irregular diameters. Nevertheless, smooth muscle cells and pericytes were present around *icap-1−/−* blood vessels (Fig. 6 E). 3D reconstruction of confocal images highlighted the dramatic malformations of tubes, which presented bulges and constrictions and partial flattening along their long axis (Video 1). Therefore, ICAP-1 is required for correct vascular morphogenesis.

Discussion

CCM proteins inhibit Rho/ROCK-dependent actomyosin contractility to stabilize VE-cadherin–dependent cell–cell junctions and maintain vascular integrity (Glading et al., 2007; Whitehead et al., 2009; Borikova et al., 2010; Stockton et al., 2010). Here, we demonstrate that increased Rho/ROCK-dependent cell contractility upon CCM1/2 loss results from higher β1 integrin activation subsequently to ICAP-1 protein destabilization. Redistribution of cellular traction forces impairs FN remodeling. In line, ultrastructural defects of the basal lamina are associated with aberrant FN remodeling around CCM lesions and ICAP-1 blood vessels. Remarkably, the aberrant ECM organization

generated by CCM1/2-depleted cells feeds back onto the cells to increase their contractility and decrease endothelial barrier function. Thus, up-regulation of β1 integrin activation participates in the progression of CCM lesions by destabilizing intercellular junctions through increased cell contractility and aberrant extracellular matrix remodeling.

CCM1 and CCM2 are involved in the fine regulation of β1 integrin activation through ICAP-1 stability

CCM1 and CCM2 regulate common processes probably as a protein complex, and their loss leads to indistinguishable phenotypes (Chan et al., 2010; Stockton et al., 2010; Boulday et al., 2011; Chan et al., 2011). ICAP-1 is a direct partner of CCM1 that binds to CCM2, and both CCM1 and ICAP-1 have been identified by mass spectrometry associated with CCM2 (Hilder et al., 2007). CCM2 sequesters ICAP-1–CCM1 in the cytoplasm (Zawistowski et al., 2005). Using siRNA silencing, knock-out animals, and ICAP-1 lifetime, we show these three proteins have stabilizing effects. Extending an in vitro study on the stabilization of ICAP-1 by CCM1 (Zhang et al., 2008), we show that ICAP-1 and CCM1 stabilize each other and are stabilized by CCM2. As observed in *ccm2*−/− embryos, ICAP-1 and CCM1 are likely lost in CCM1 and CCM2 lesions, providing a mechanistic rationale for their indistinguishable phenotypes.

ICAP-1 keeps β1 integrin in its inactivated form by competing with kindlin and talin for binding to β1 integrin cytoplasmic tail (Bouvard et al., 2003; Millon-Frémillon et al., 2008; Brunner et al., 2011). Here, we show that CCM1 and CCM2 control β1 integrin activation. In the pathological condition upon CCM1/2 loss, β1 integrin overactivation most likely comes from the destabilization of ICAP-1 protein. A recent article suggests on the contrary that loss of CCM1 leads to inhibition of β1 integrin activation (Liu et al., 2013). In support of this, no ICAP-1 destabilization is observed upon CCM1 loss. This discrepancy with our results probably comes from their use of an endothelial cell line EA.hy926 instead of primary HUVECs. This permanent cell line is a fusion between HUVECs and a human carcinoma cell line (Edgell et al., 1983). EA.hy926 cells express much more ICAP-1 and CCM1 than HUVECs and, inversely, dramatically less β1 integrin on their cell surface (unpublished data). These disruptions in the balance between the three partners are likely to have profound artifact effects on β1 integrin activation. In the physiological condition when both ICAP-1 and CCM1 are present, the emerging picture is that the CCM1–ICAP-1 complex is presented to β1 integrin. ICAP-1 binds to β1 integrin releasing CCM1 (Liu et al., 2013), which can then regulate cell–cell junction formation and/or stabilization.

CCM1/2 proteins regulate intracellular tension and ECM remodeling through control of β1 integrin activation

Actomyosin contractility is up-regulated in CCM-depleted cells as a result of increased RhoA activation and ROCK-dependent myosin phosphorylation (Whitehead et al., 2009; Borikova et al., 2010; Stockton et al., 2010). It is known that β1 integrin–dependent cell adhesion to ECM is a signal for RhoA activation

and cell contractility (Huveneers et al., 2008). Here, we show that β1 integrin is required for increased RhoA activation upon CCM1/2 loss and for the appearance of actin stress fibers. Several GEFs and GAPs of RhoA are regulated by β1 integrin and mechanical forces (Guilluy et al., 2011); further studies should determine the ones involved in this context. We propose that, in physiological condition, the CCM complex maintains β1 integrin activation low to block RhoA-dependent cell contractility, and to prevent its deleterious effects on cell–cell junction stability, cell polarity, and in fine the quiescence of the vessel.

As a result of dysregulated β1 integrin activation and cell contractility, FN fibrillogenesis does not proceed normally upon CCM protein loss. Depleted cells generate linear and parallel FN fibers instead of the interlaced and woven fibers of CT cells. As the polymerization of FN in long and wavy fibers requires the propagation of peripheral forces toward the cell body (Lemmon et al., 2009), dysregulation of the spatio-temporal propagation of forces in cells silenced for ICAP-1 or CCM1/2 likely causes abnormal FN fibrillogenesis.

In vivo FN deposition around mouse CCM lesions and ICAP-1–deficient blood vessels is consistently abnormal. It is composed of more numerous FN fibers over a higher background of soluble FN dimers. FN fibers provide a scaffold for matrix proteins, including fibrillar collagens and collagen IV, and orchestrate their assembly (Sottile et al., 2007; Stratman et al., 2009). Fibers of collagen III colocalized with the FN fibrils around CCM lesions, whereas they were almost absent around normal blood vessels. Moreover, these remodeling defects are associated with increased production of EDA cFN. Cellular FN variants EDA and EDB are markers of angiogenic vessels during embryonic development or tumoral angiogenesis (Rybak et al., 2007; Van Obberghen-Schilling et al., 2011; Booth et al., 2012). Collagen III, EDA, and EDB cFN are also expressed during fibrosis (Theodossiou et al., 2006; Booth et al., 2012). FN-driven fibrosis around CCM lesions could lead to an inflammatory response and damage the peripheral neuronal tissue (Khan et al., 2012). These morphological ECM defects are correlated with abnormal ultrastructure of the basal lamina and interstitial ECM. We found multilayering of the basal lamina and enlargement of the interstitial ECM in ICAP-1–deficient vessels. This is reminiscent of human and mouse CCM lesions (Wong et al., 2000; Clatterbuck et al., 2001; Chan et al., 2011; McDonald et al., 2011) and points to ICAP-1 dysfunctions as a cause for abnormal basal lamina around CCM-deficient blood vessels.

ICAP-1 deficiency leads to vascular defects that partially recapitulate those in endothelial CCM1/2-deficient mice. Contrary to *ccm*1 and *ccm*2 constitutive or endothelial-specific knock-out mice, vascular defects upon ICAP-1 deficiency do not lead to developmental lethality or cerebral cavernoma lesions (Whitehead et al., 2004, 2009; Boulday et al., 2009; Kleaveland et al., 2009). As ICAP-1 can complex with CCM1 or β1 integrin (Liu et al., 2013), it is likely that ICAP-1 and CCM1 have common and distinct functions. Contrary to *ccm*1 and *ccm*2 knock-out mice, for which both CCM1 and ICAP-1 are lost, CCM1 is present in ICAP-1–deficient animals, to a lesser extent though than in wild-type animals (25% of wild type). It is possible that the remaining level of CCM1 protein in ICAP-1−/− mice is
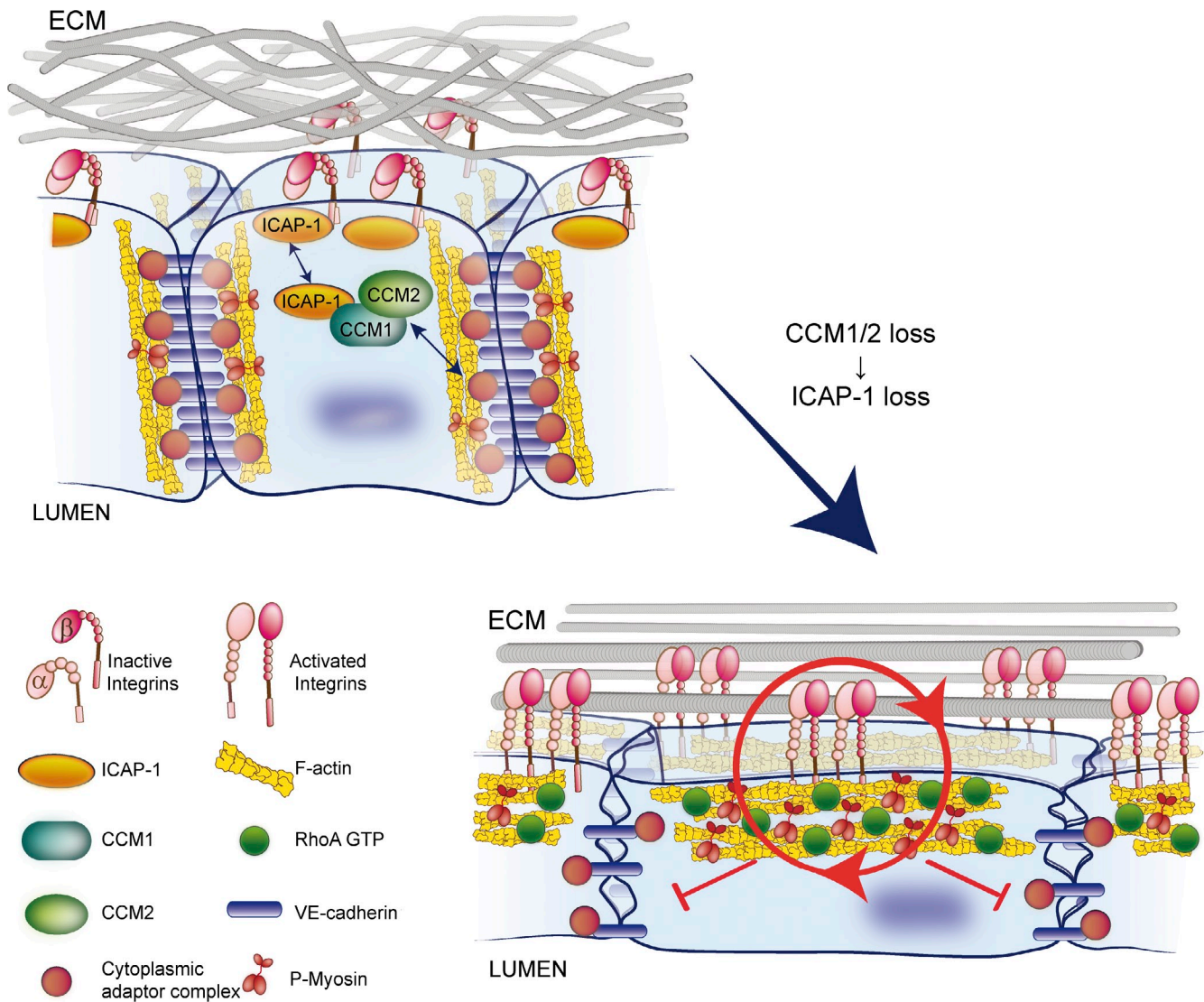
Figure 8. **β1 activation upon loss in CCM1 or 2 drives a loop between endothelial cell contractility and ECM with deleterious effect on cell–cell junctions.** In a quiescent vessel, ICAP-1 maintains low β1 integrin activation. Endothelial cells are well joined and VE-cadherin adherens junctions are stabilized by a cytoplasmic adaptor complex that recruits junctional actomyosin cytoskeleton. Upon CCM1 or CCM2 depletion, ICAP-1 protein is destabilized and lost. β1 integrin is activated and activates in turn RhoA/ROCK-dependent actin stress fiber formation. Increased β1 integrin activation and cell contractility result in aberrant remodeling of ECM in linear and parallel fibers onto which cells spread and flatten. A self-sustaining mechanical loop is initiated that increases intra- and external tensions destabilizing cell–cell junctions.

sufficient for it to perform its ICAP-1–independent functions, allowing developmental angiogenesis to proceed and preventing the formation of CCM lesions in born animals.

Cell–cell junctions are regulated by a β1 integrin–dependent loop between microenvironment and cell contractility downstream of CCM–ICAP-1 complex

Increased cellular contractility is deleterious for VE-cadherin–dependent adherens junctions, endothelial barrier function, and CCM lesion formation. RhoA or ROCK inhibitors decrease vascular leaks in CCM1 and CCM2 heterozygous animals (Whitehead et al., 2009; Stockton et al., 2010) and slow down the maturation of CCM lesions from isolated caverns to large multi-cavernous hemorrhagic structures (McDonald et al., 2012). Interestingly, actin dynamics has a prominent role in the cross talk between

cell–cell and cell–ECM adhesion (Burute and Thery, 2012). Because β1 integrin is a master organizer of actin in CCM1/2-depleted cells, it represents a good therapeutic target to decrease vascular leak in CCM lesions. Several inhibitors of activated β1 integrin under clinical trials in cancer therapy (Barkan and Chambers, 2011) could be tested on the CCM1/2-inducible mouse models.

Moreover, we show that aberrant ECM remodeling in an array of straight FN and collagen fibers is linked to increased cell contractility and β1 integrin–dependent adhesion upon CCM1/2 depletion. Interestingly, highly aligned and organized collagen fibers are also found around tumors in vivo and generate a stiff microenvironment favorable for tumor cell invasiveness (Gaggioli et al., 2007; Provenzano et al., 2008; Goetz et al., 2011). Further experiments are ongoing to determine whether such ECM remodeling stiffens the microenvironment around CCM lesions and

ICAP-1–deficient blood vessels. Using decellularized matrices remodeled by CCM-depleted endothelial cells, we show that the structure of the CCM1/2 KD matrices was responsible for increased cell contractility and decreased barrier function of the endothelial monolayer. It is likely that the higher external tension imposed by the ECM feeds back onto the cells, enhancing their internal tension, and creates a self-sustaining mechanical loop as for tumoral cells (DuFort et al., 2011; Goetz et al., 2011). This loop is deleterious for the stability of VE-cadherin cell–cell junctions (Fig. 8). It has been shown accordingly that increased ECM stiffness inhibits cell–cell junction formation (Maruthamuthu et al., 2011; Tseng et al., 2012) and enhances the response of the endothelium to permeability factors such as thrombin (Krishnan et al., 2011). We propose that β1 integrin–dependent ECM remodeling is an additional cue to the progression of CCM lesions. Lesions are mosaics of wild-type and mutated endothelial cells (Pagenstecher et al., 2009). By mid-range propagation, this defect in ECM organization would have deleterious effects on mutant and adjacent wild-type endothelial cells and could be involved in the maturation of CCM lesions from small isolated caverns to large multi-cavernous hemorrhagic structures (McDonald et al., 2011). Consistent with this model, pMLC staining becomes more intense upon CCM maturation, and ROCK inhibition by Fasudil reduces the size of mouse CCM1 lesions and their maturation into hemorrhagic lesions (McDonald et al., 2012). Therefore, inhibition of FN fibrillogenesis with competing peptides or blocking antibodies could also be tested on the CCM1/2-inducible mouse models.

Altogether, our data show for the first time that in addition to regulating cell–cell adhesion, CCM proteins control the biomechanical dialogue of the endothelial cell with its surrounding ECM through β1 integrin activation, and that this dialogue impacts cell–cell adhesion. The role of the CCM proteins in the cross talks between these different signaling pathways should be further studied to have a comprehensive view of their function and to set up therapeutic treatments.

Materials and methods

Reagents and antibodies
Bovine plasma fibronectin was purified by affinity chromatography of plasma on columns containing covalently coupled denatured collagen, and the bound fibronectin was eluted by 4 M urea according to the method already described (Albigès-Rizo et al., 1995; Engvall and Ruoslahti, 1977). Rat tail collagen I was from BD. EBM medium and HUVEC growth factors were from Lonza. Table S1 lists the commercial antibodies used. Rabbit anti–ICAP-1 serum was raised by immunizing rabbits with purified recombinant His-tagged ICAP-1 (aa 1–150) as antigen (Millon-Frémillon et al., 2008). Polyclonal rabbit anti-CCM1 was raised against the recombinant CCM1 fragment 1–400 aa produced in *Escherichia coli* and affinity purified. A second polyclonal CCM1 antibody, in Lampugnani et al. (2010), was also used. CCM2 polyclonal antibody was as in Boulday et al. (2011). The pQE30-FUD plasmid was a gift from D. Mosher (University of Wisconsin-Madison, Madison, WI). Recombinant FUD was produced in *E. coli* and affinity purified.

Mouse strain
Mice with a targeted mutation on the ICAP-1 locus (Itgb1bp1[tm1ref]) were genotyped as previously reported (Bouvard et al., 2007). Mice were bred in a CD1 background and adult homozygous mice (2–4 mo) were generated by crossing heterozygous mice. The present study conforms to the Guide for the Care and Use of Laboratory Animals published by the National Institutes of Health (Bethesda, MD); the protocol was approved by

the Animal Care and Use Committee (Comité d'éthique en expérimentation animale de Grenoble). The iCCM1 and iCCM2 P1 pups received a single intragastric injection of 20 µg tamoxifen as in Boulday et al. (2011). Tamoxifen (Sigma-Aldrich) was diluted in sunflower oil/10% ethanol.

Immunohistochemistry
For ear whole-mount staining, the ears were dissected out with forceps, separating the dorsal and ventral leaflets and fixed overnight in 4% paraformaldehyde (Lebrin et al., 2010). The dorsal leaflet was processed for immunostaining with primary antibodies listed in Table S1. After rinsing, coverslips were incubated with an appropriate Alexa Fluor–conjugated secondary antibody. The tissues were mounted in Mowiol/DAPI solution. Frozen brain sections (16 µm) from iCCM1 and iCCM2 were post-fixed in acetone, blocked with BSA and goat serum, and immunostained with PECAM, FN, and collagen III as described previously (Boulday et al., 2011). Z-stack images (0.5-µm step) were acquired on a confocal microscope (LSM 510; Carl Zeiss) with a Plan Apochromat 63×/1.4 NA oil objective, DICIII, WD 180. Z-stack projections were done using the LSM program.

Quantifications of vessel branching and diameters
Vessel branching was quantified on photographs of intestine mesenteric veins of *icap-1+/+* and *icap-1−/−* mice using ImageJ software (National Institutes of Health). The final number of branches was counted for each initial mesenteric vein. Vessel diameters were determined on projections of confocal z-stacks of ear whole-mount–stained blood vessels with PECAM at 20×. Images were normalized and more than 100 diameters per mouse were measured using ImageJ software.

In vivo tracer diffusion imaging
Mice were anesthetized by intraperitoneal injection of ketamine (100 mg/kg body weight) and domitor (8 mg/kg body weight) and were placed supine on the platform of the MacroFluo imaging system (Leica) with their ear gently stretched under a microscope slide. A mixture of lysine-fixable 70 kD dextran-FITC and 10 kD dextran–Alexa Fluor 546 (Invitrogen; 0.1 mg of each in 200 µl of PBS) was injected intravenously into their tail vein. Fluorescent images were acquired continuously for 15 min by a CCD camera (ORCA II-BT-512G; Hamamatsu Photonics). Excitation was performed at 480 nm (BP 480/40-nm filter) and 546 nm (515–560 nm). Fluorescence emission was detected simultaneously in the BP 527/30-nm and LP 590-nm channels for FITC and Alexa Fluor 546, respectively.

Transmission electron microscopy
Samples were fixed overnight at 4°C in 2.5% glutaraldehyde, 2% paraformaldehyde in sodium cacodylate buffer 0.1 M, pH 7.4. After three washes in 0.1 M sodium cacodylate, pH 7.4, specimens were post-fixed in 1% osmium tetroxide, 0.1 M cacodylate, pH 7.4, for 45 min, dehydrated in a graded series of ethanol, and embedded in epoxy resin. Ultra-thin 70-nm sections stained with uranyl acetate and lead citrate were observed with an electron microscope (model CM120, Philips; Centre Technologique des Microstructures, University Lyon 1, Villeurbanne, France).

Cell culture and transfection
HUVECs were obtained from Lonza and grown in EGM-2 media supplemented with 100 U/ml penicillin and 100 µg/ml streptomycin at 37°C in a 5% CO2-humidified chamber according to the manufacturer's instructions. HUVECs (1.5 × 10^6 cells) were transfected twice at 24-h intervals with 20 nM siRNA and 45 µl lipofectamine RNAi max (Invitrogen) according to the manufacturer's instructions. Cells were used the day after the second round of transfection. For β1 or β3 integrin silencing, 20 nM of siGENOME smart pool siRNA (Thermo Fisher Scientific) were used in combination with CT, ICAP-1, CCM1, or CCM2 siRNA and three rounds of transfection were performed. Table S2 shows the sequences of siRNA duplexes for CT, ICAP-1, and CCM1 (Eurogentec). CCM2 siRNA are an ON-TARGET smart pool from Thermo Fisher Scientific.

CHO (Chinese hamster ovary) cells were grown in DMEM (PAA) and transfected with Exgen (Euromedex) following the manufacturer's instructions, using pCDNA3-ICAP-1 vector with or without pcDNA-FLAG-CCM1 wild-type or N192-Y195/AA mutant (Béraud-Dufour et al., 2007).

Lifetime of ICAP-1 protein measurement
Transfected CHO cells were incubated with cycloheximide (Sigma-Aldrich) at 100 µg/ml with or without 10 µM of MG132. After indicated times, cells were then lysed in RIPA buffer and protein concentration was measured by BCA assay. Total proteins (20 µg) were run on SDS-PAGE and immunoblotted as below.

Quantitative RT-PCR (qPCR)

Total RNA was extracted from cells using the NucleoSpin RNA II kit (Macherey-Nagel) according to the manufacturer's instructions. RNA (1 µg) was reverse transcribed using the SuperScript VILO kit (Life Technologies). Quantitative real-time PCR was performed with GoTaq[R] QPCR Master Mix (Promega) in a 25-µl reaction on a thermal cycler (C-1000 Touch; Bio-Rad Laboratories). Product sizes were controlled by DNA gel electrophoresis and the melt curves were evaluated using CFX Manager (Bio-Rad Laboratories). Ct values were determined with the same software, and normalization was done with the house keeping genes GAPDH, RELA, or ATP50, yielding very similar results. Expression levels of each target gene in the siRNA cells were calculated with GAPDH as reference gene and compared with control. All PCR primer sequences are listed in Table S3.

Cell spreading and immunofluorescence

Transfected cells were trypsinized, treated with 1 mg/ml trypsin inhibitor (Sigma-Aldrich), and incubated in serum-free EBM-2/1% BSA for 30 min at 37°C. Sparse HUVECs (10^4 cells) were incubated for different times at 37°C in 24-well plates on slides coated with 0.3 µg/cm^2 (1 µg/ml) of FN in EBM-2 media containing 5% FN-depleted serum to study inside-out signaling effect of protein deletion on cell adhesion to ECM (Millon-Frémillon et al., 2008), and then fixed. Confluent HUVECs (3×10^5 cells) were seeded in 24-well plates on slides coated with 20 µg/ml FN and incubated for 48 h in supplemented EGM-2 media, then for another 24 h in basal EBM-2 containing 0.3% BSA. Cells were immunostained as already described (Millon-Frémillon et al., 2008). In brief, cells were fixed with 4% PFA, permeabilized with 0.2% Triton X-100, and incubated with appropriate primary antibodies (see list in Table S1). After rinsing, coverslips were incubated with an appropriate Alexa Fluor–conjugated secondary antibody. The cells were mounted in Mowiol/DAPI solution and imaged on a microscope (Axio Imager M2; Carl Zeiss) equipped with a Plan Apochromat 63×/1.4 NA oil objective, DICIII, WD 190, and a camera (6.45 × 6.45 µm, −10°C BRT, ~8 im/s; AxioCam MRc, Carl Zeiss).

Quantifications of the percentage of cells displaying central β1 integrin–containing FA or transversal actin fibers above the nucleus were done on more than 100 cells.

Measurement of β1 integrin activation by flow cytometry

Transfected HUVECs were harvested after trypsin treatment and incubated at 37°C for 15 min with 10 µM blebbistatin and then, with or without 0.5 mM MnCl$_2$ for 15 min on ice. 9EG7 antibody was added to the cell suspension at 1:100 and incubated for 30 min on ice. Cells were washed and labeled with fluorophore-conjugated secondary antibody (Alexa Fluor 488 goat anti–rat). After final wash, cells were fixed in 4% PFA for 10 min on ice, washed in PBS, and then analyzed using a flow cytometer (LSR II; BD). The integrin index activation was calculated as the mean fluorescence intensity of 9EG7 staining (active β1 integrin) divided by the mean fluorescence of 9EG7 staining in the presence of MnCl$_2$ (total β1 integrin). Results were expressed as percentage of activated β1 integrin in CT cells.

Measurement of RhoA activation

HUVECs were transfected by three rounds of siRNA against ICAP-1 or CCM1 or CCM2 in the presence or not of β1 integrin siRNA. Confluent cells were then serum starved overnight and RhoG-LISA or Rhotekin pull-down assays (Cytoskeleton, Inc.) were performed as recommended by the manufacturer.

Traction force microscopy

Traction force microscopy calculations were performed as described previously (Tseng et al., 2011). A home-made Fourier transform traction cytometry (FTTC) algorithm with zeroth-order regularization computed cellular traction forces from the measured substrate displacements. These are determined from images of fluorescent beads embedded inside the gel network with and without the adherent cell. After correction for experimental drift, fluorescent beads are tracked to obtain a displacement field with high spatial resolution. The final displacement field is obtained on a regular grid with 0.84-µm spacing by linear interpolation. Force reconstruction was conducted with the assumption that the substrate is a linear elastic half-space. Traction force microscopy experiments were performed using a microscope (Ti-E; Nikon) equipped with an incubator maintaining the temperature at 37°C, mounted with a CCD camera (CoolSNAP; Roper Scientific) and driven with microManager (http://www.micro-manager.org). Cells were imaged with a Nikon 63× air objective lens (NA 1.4). Microbeads used for TFM were 200-nm Dragon Green beads provided by Bangs Laboratories, Inc.

Preparation of decellularized remodeled matrices

60,000 silenced HUVECs were seeded on slides coated with FN at 6 µg/cm^2 and cultured for 48 h under normoxia (3% O$_2$) in EGM-2 media. In FUD conditions, recombinant FUD peptide was added at a final concentration of 500 nM in the media and added again 24 h after. Cells were then lysed with 0.5% Triton X-100 in PBS for 15 min on ice. Nuclei were removed by incubation with 50 mM ammonium hydroxide for 15 min on ice. Resulting decellularized matrices were extensively washed with PBS and used for subsequent plating with naive HUVECs.

Quantification of the thickness of β-catenin junctional staining

HUVECs were seeded at confluency and cultured for 48 h in EGM-2 media containing 5% FN-depleted serum. Images were acquired on a microscope (Axio Imager; Carl Zeiss) at 40×. Surface and length of the junctional β-catenin staining for the entire image were measured using the integrated morphometric analyses of MetaMorph application and means were calculated from values of five images. The thickness of β-catenin staining was obtained with the ratio surface/length.

Electrical impedance measurements

The xCELLigence real-time cell analyzer (RTCA) system (Roche) was used to measure electrical impedance over time. Changes in impedance of confluent endothelial cells reflect changes in barrier function (Atienza et al., 2006). Remodeled matrices were produced in wells of E-plates 16 as described in the section dedicated to the preparation of decellularized remodeled matrices. 60,000 naive HUVECs were seeded on these plates (4 wells per condition) in EGM-2 media containing 5% FN-depleted serum. Cell index was measured every 10 min. Normalized cell index was calculated after cells had adhered and spread (1 h 30 min time point).

Western blot analysis

Cells or ground-frozen mouse livers were lysed in Laemmli buffer, run on SDS-PAGE, and transferred on PVDF membranes. Immunological detection was achieved with HRP-conjugated secondary antibody. Peroxidase activity was visualized by ECL (West Pico signal; Thermo Fisher Scientific) using a ChemiDoc MP imaging system (Bio-Rad Laboratories). Densitometric quantification of the bands was performed using the Image Laboratory program (Bio-Rad Laboratories).

Statistical analysis

Comparisons between groups were analyzed by Student's two-tailed paired t test with a significance level of $P < 0.05$. Alternatively, data were analyzed for statistical significance by GLMM with a Tukey's multiple comparison test.

Online supplemental material

Fig. S1 shows ICAP-1 and CCM1 protein contents in CCM2 embryos and ICAP-1 livers, respectively. Fig. S2 shows colocalization of talin with β1 integrin–dependent focal adhesions in ICAP-1–, CCM1-, and CCM2-depleted HUVECs. Fig. S3 shows the effect of β1 integrin silencing on RhoA activation and actin contractility of sparse HUVECs depleted in ICAP-1, CCM1, or CCM2. Fig. S4 shows VE-cadherin and β catenin staining on confluent HUVECs silenced for ICAP-1, CCM1, and CCM2. Fig. S5 shows pleiotropic vascular defects in ICAP-1–deficient mice associated with defects in the ultrastructure of the basal lamina. Video 1 shows 360° rotation movies around ICAP-1+/+ and ICAP-1−/− blood vessels. Online supplemental material is available at http://www.jcb.org/cgi/content/full/jcb .201303044/DC1. Additional data are available in the JCB DataViewer at http://dx.doi.org/10.1083/jcb.201303044.dv.

References

Abraham, S., N. Kogata, R. Fässler, and R.H. Adams. 2008. Integrin beta1 subunit controls mural cell adhesion, spreading, and blood vessel wall stability. *Circ. Res.* 102:562–570. http://dx.doi.org/10.1161/CIRCRESAHA.107.167908

Albigès-Rizo, C., P. Frachet, and M.R. Block. 1995. Down regulation of talin alters cell adhesion and the processing of the alpha 5 beta 1 integrin. *J. Cell Sci.* 108:3317–3329.

Atienza, J.M., N. Yu, S.L. Kirstein, B. Xi, X. Wang, X. Xu, and Y.A. Abassi. 2006. Dynamic and label-free cell-based assays using the real-time cell electronic sensing system. *Assay Drug Dev. Technol.* 4:597–607. http://dx.doi.org/10.1089/adt.2006.4.597

Barkan, D., and A.F. Chambers. 2011. β1-integrin: a potential therapeutic target in the battle against cancer recurrence. *Clin. Cancer Res.* 17:7219–7223. http://dx.doi.org/10.1158/1078-0432.CCR-11-0642

Bazzoni, G., D.T. Shih, C.A. Buck, and M.E. Hemler. 1995. Monoclonal antibody 9EG7 defines a novel beta 1 integrin epitope induced by soluble ligand and manganese, but inhibited by calcium. *J. Biol. Chem.* 270:25570–25577. http://dx.doi.org/10.1074/jbc.270.30.17784

Béraud-Dufour, S., R. Gautier, C. Albiges-Rizo, P. Chardin, E. Faurobert, and S. Béraud-Dufour. 2007. Krit 1 interactions with microtubules and membranes are regulated by Rap1 and integrin cytoplasmic domain associated protein-1. *FEBS J.* 274:5518–5532. http://dx.doi.org/10.1111/j.1742-4658.2007.06068.x

Boettner, B., and L. Van Aelst. 2009. Control of cell adhesion dynamics by Rap1 signaling. *Curr. Opin. Cell Biol.* 21:684–693. http://dx.doi.org/10.1016/j.ceb.2009.06.004

Booth, A.J., S.C. Wood, A.M. Cornett, A.A. Dreffs, G. Lu, A.F. Muro, E.S. White, and D.K. Bishop. 2012. Recipient-derived EDA fibronectin promotes cardiac allograft fibrosis. *J. Pathol.* 226:609–618. http://dx.doi.org/10.1002/path.3010

Borikova, A.L., C.F. Dibble, N. Sciaky, C.M. Welch, A.N. Abell, S. Bencharit, and G.L. Johnson. 2010. Rho kinase inhibition rescues the endothelial cell cerebral cavernous malformation phenotype. *J. Biol. Chem.* 285:11760–11764. http://dx.doi.org/10.1074/jbc.C109.097220

Boulday, G., A. Blécon, N. Petit, F. Chareyre, L.A. Garcia, M. Niwa-Kawakita, M. Giovannini, and E. Tournier-Lasserve. 2009. Tissue-specific conditional CCM2 knockout mice establish the essential role of endothelial CCM2 in angiogenesis: implications for human cerebral cavernous malformations. *Dis. Model. Mech.* 2:168–177. http://dx.doi.org/10.1242/dmm.001263

Boulday, G., N. Rudini, L. Maddaluno, A. Blécon, M. Arnould, A. Gaudric, F. Chapon, R.H. Adams, E. Dejana, and E. Tournier-Lasserve. 2011. Developmental timing of CCM2 loss influences cerebral cavernous malformations in mice. *J. Exp. Med.* 208:1835–1847. http://dx.doi.org/10.1084/jem.20110571

Bouvard, D., L. Vignoud, S. Dupé-Manet, N. Abed, H.N. Fournier, C. Vincent-Monegat, S.F. Retta, R. Fassler, and M.R. Block. 2003. Disruption of focal adhesions by integrin cytoplasmic domain-associated protein-1 alpha. *J. Biol. Chem.* 278:6567–6574. http://dx.doi.org/10.1074/jbc.M211258200

Bouvard, D., A. Millon-Fremillon, S. Dupe-Manet, M.R. Block, and C. Albiges-Rizo. 2006. Unraveling ICAP-1 function: toward a new direction? *Eur. J. Cell Biol.* 85:275–282. http://dx.doi.org/10.1016/j.ejcb.2005.10.005

Bouvard, D., A. Aszodi, G. Kostka, M.R. Block, C. Albigès-Rizo, and R. Fässler. 2007. Defective osteoblast function in ICAP-1-deficient mice. *Development.* 134:2615–2625. http://dx.doi.org/10.1242/dev.008807

Brunner, M., A. Millon-Frémillon, G. Chevalier, I.A. Nakchbandi, D. Mosher, M.R. Block, C. Albigès-Rizo, and D. Bouvard. 2011. Osteoblast mineralization requires beta1 integrin/ICAP-1-dependent fibronectin deposition. *J. Cell Biol.* 194:307–322. http://dx.doi.org/10.1083/jcb.201007108

Brütsch, R., S.S. Liebler, J. Wüstehube, A. Bartol, S.E. Herberich, M.G. Adam, A. Telzerow, H.G. Augustin, and A. Fischer. 2010. Integrin cytoplasmic domain-associated protein-1 attenuates sprouting angiogenesis. *Circ. Res.* 107:592–601. http://dx.doi.org/10.1161/CIRCRESAHA.110.217257

Burute, M., and M. Thery. 2012. Spatial segregation between cell-cell and cell-matrix adhesions. *Curr. Opin. Cell Biol.* 24:628–636. http://dx.doi.org/10.1016/j.ceb.2012.07.003

Chan, A.C., D.Y. Li, M.J. Berg, and K.J. Whitehead. 2010. Recent insights into cerebral cavernous malformations: animal models of CCM and the human phenotype. *FEBS J.* 277:1076–1083. http://dx.doi.org/10.1111/j.1742-4658.2009.07536.x

Chan, A.C., S.G. Drakos, O.E. Ruiz, A.C. Smith, C.C. Gibson, J. Ling, S.F. Passi, A.N. Stratman, A. Sacharidou, M.P. Revelo, et al. 2011. Mutations in 2 distinct genetic pathways result in cerebral cavernous malformations in mice. *J. Clin. Invest.* 121:1871–1881. http://dx.doi.org/10.1172/JCI44393

Chang, D.D., C. Wong, H. Smith, and J. Liu. 1997. ICAP-1, a novel beta1 integrin cytoplasmic domain-associated protein, binds to a conserved and functionally important NPXY sequence motif of beta1 integrin. *J. Cell Biol.* 138:1149–1157. http://dx.doi.org/10.1083/jcb.138.5.1149

Clark, K., R. Pankov, M.A. Travis, J.A. Askari, A.P. Mould, S.E. Craig, P. Newham, K.M. Yamada, and M.J. Humphries. 2005. A specific alpha5beta1-integrin conformation promotes directional integrin translocation and fibronectin matrix formation. *J. Cell Sci.* 118:291–300. http://dx.doi.org/10.1242/jcs.01623

Clatterbuck, R.E., C.G. Eberhart, B.J. Crain, and D. Rigamonti. 2001. Ultrastructural and immunocytochemical evidence that an incompetent blood-brain barrier is related to the pathophysiology of cavernous malformations. *J. Neurol. Neurosurg. Psychiatry.* 71:188–192. http://dx.doi.org/10.1136/jnnp.71.2.188

Colombelli, J., A. Besser, H. Kress, E.G. Reynaud, P. Girard, E. Caussinus, U. Haselmann, J.V. Small, U.S. Schwarz, and E.H. Stelzer. 2009. Mechanosensing in actin stress fibers revealed by a close correlation between force and protein localization. *J. Cell Sci.* 122:1665–1679. http://dx.doi.org/10.1242/jcs.042986

Cunningham, K., Y. Uchida, E. O'Donnell, E. Claudio, W. Li, K. Soneji, H. Wang, Y.S. Mukouyama, and U. Siebenlist. 2011. Conditional deletion of Ccm2 causes hemorrhage in the adult brain: a mouse model of human cerebral cavernous malformations. *Hum. Mol. Genet.* 20:3198–3206. http://dx.doi.org/10.1093/hmg/ddr225

DuFort, C.C., M.J. Paszek, and V.M. Weaver. 2011. Balancing forces: architectural control of mechanotransduction. *Nat. Rev. Mol. Cell Biol.* 12:308–319. http://dx.doi.org/10.1038/nrm3112

Edgell, C.J., C.C. McDonald, and J.B. Graham. 1983. Permanent cell line expressing human factor VIII-related antigen established by hybridization. *Proc. Natl. Acad. Sci. USA.* 80:3734–3737. http://dx.doi.org/10.1073/pnas.80.12.3734

Engvall, E., and E. Ruoslahti. 1977. Binding of soluble form of fibroblast surface protein, fibronectin, to collagen. *Int. J. Cancer.* 20:1–5. http://dx.doi.org/10.1002/ijc.2910200102

Faurobert, E., and C. Albiges-Rizo. 2010. Recent insights into cerebral cavernous malformations: a complex jigsaw puzzle under construction. *FEBS J.* 277:1084–1096. http://dx.doi.org/10.1111/j.1742-4658.2009.07537.x

Gaggioli, C., S. Hooper, C. Hidalgo-Carcedo, R. Grosse, J.F. Marshall, K. Harrington, and E. Sahai. 2007. Fibroblast-led collective invasion of carcinoma cells with differing roles for RhoGTPases in leading and following cells. *Nat. Cell Biol.* 9:1392–1400. http://dx.doi.org/10.1038/ncb1658

Glading, A., J. Han, R.A. Stockton, and M.H. Ginsberg. 2007. KRIT-1/CCM1 is a Rap1 effector that regulates endothelial cell cell junctions. *J. Cell Biol.* 179:247–254. http://dx.doi.org/10.1083/jcb.200705175

Goetz, J.G., S. Minguet, I. Navarro-Lérida, J.J. Lazcano, R. Samaniego, E. Calvo, M. Tello, T. Osteso-Ibáñez, T. Pellinen, A. Echarri, et al. 2011. Biomechanical remodeling of the microenvironment by stromal caveolin-1 favors tumor invasion and metastasis. *Cell.* 146:148–163. http://dx.doi.org/10.1016/j.cell.2011.05.040

Guilluy, C., V. Swaminathan, R. Garcia-Mata, E.T. O'Brien, R. Superfine, and K. Burridge. 2011. The Rho GEFs LARG and GEF-H1 regulate the mechanical response to force on integrins. *Nat. Cell Biol.* 13:722–727. http://dx.doi.org/10.1038/ncb2254

Hilder, T.L., M.H. Malone, S. Bencharit, J. Colicelli, T.A. Haystead, G.L. Johnson, and C.C. Wu. 2007. Proteomic identification of the cerebral cavernous malformation signaling complex. *J. Proteome Res.* 6:4343–4355. http://dx.doi.org/10.1021/pr0704276

Huttenlocher, A., M.H. Ginsberg, and A.F. Horwitz. 1996. Modulation of cell migration by integrin-mediated cytoskeletal linkages and ligand-binding affinity. *J. Cell Biol.* 134:1551–1562. http://dx.doi.org/10.1083/jcb.134.6.1551

Huveneers, S., and E.H. Danen. 2009. Adhesion signaling - crosstalk between integrins, Src and Rho. *J. Cell Sci.* 122:1059–1069. http://dx.doi.org/10.1242/jcs.039446

Huveneers, S., H. Truong, R. Fässler, A. Sonnenberg, and E.H. Danen. 2008. Binding of soluble fibronectin to integrin alpha5 beta1 - link to focal adhesion redistribution and contractile shape. *J. Cell Sci.* 121:2452–2462. http://dx.doi.org/10.1242/jcs.033001

Hynes, R.O. 2002. Integrins: bidirectional, allosteric signaling machines. *Cell.* 110:673–687. http://dx.doi.org/10.1016/S0092-8674(02)00971-6

Khan, M.M., C. Gandhi, N. Chauhan, J.W. Stevens, D.G. Motto, S.R. Lentz, and A.K. Chauhan. 2012. Alternatively-spliced extra domain A of fibronectin promotes acute inflammation and brain injury after cerebral ischemia in mice. *Stroke.* 43:1376–1382. http://dx.doi.org/10.1161/STROKEAHA.111.635516

Kleaveland, B., X. Zheng, J.J. Liu, Y. Blum, J.J. Tung, Z. Zou, S.M. Sweeney, M. Chen, L. Guo, M.M. Lu, et al. 2009. Regulation of cardiovascular development and integrity by the heart of glass-cerebral cavernous malformation protein pathway. *Nat. Med.* 15:169–176. http://dx.doi.org/10.1038/nm.1918

Krishnan, R., D.D. Klumpers, C.Y. Park, K. Rajendran, X. Trepat, J. van Bezu, V.W. van Hinsbergh, C.V. Carman, J.D. Brain, J.J. Fredberg, et al. 2011.

Substrate stiffening promotes endothelial monolayer disruption through enhanced physical forces. *Am. J. Physiol. Cell Physiol.* 300:C146–C154. http://dx.doi.org/10.1152/ajpcell.00195.2010

Lampugnani, M.G., F. Orsenigo, N. Rudini, L. Maddaluno, G. Boulday, F. Chapon, and E. Dejana. 2010. CCM1 regulates vascular-lumen organization by inducing endothelial polarity. *J. Cell Sci.* 123:1073–1080. http://dx.doi.org/10.1242/jcs.059329

Larsen, M., V.V. Artym, J.A. Green, and K.M. Yamada. 2006. The matrix reorganized: extracellular matrix remodeling and integrin signaling. *Curr. Opin. Cell Biol.* 18:463–471. http://dx.doi.org/10.1016/j.ceb.2006.08.009

Lebrin, F., S. Srun, K. Raymond, S. Martin, S. van den Brink, C. Freitas, C. Breant, T. Mathivet, B. Larrivee, J.-L. Thomas, et al. 2010. Thalidomide stimulates vessel maturation and reduces epistaxis in individuals with hereditary hemorrhagic telangiectasia. *Nat. Med.* 16:420–428.

Lemmon, C.A., C.S. Chen, and L.H. Romer. 2009. Cell traction forces direct fibronectin matrix assembly. *Biophys. J.* 96:729–738. http://dx.doi.org/10.1016/j.bpj.2008.10.009

Liu, W., K.M. Draheim, R. Zhang, D.A. Calderwood, and T.J. Boggon. 2013. Mechanism for KRIT1 release of ICAP1-mediated suppression of integrin activation. *Mol. Cell.* 49:719–729. http://dx.doi.org/10.1016/j.molcel.2012.12.005

Maruthamuthu, V., B. Sabass, U.S. Schwarz, and M.L. Gardel. 2011. Cell-ECM traction force modulates endogenous tension at cell-cell contacts. *Proc. Natl. Acad. Sci. USA.* 108:4708–4713. http://dx.doi.org/10.1073/pnas.1011123108

McDonald, D.A., R. Shenkar, C. Shi, R.A. Stockton, A.L. Akers, M.H. Kucherlapati, R. Kucherlapati, J. Brainer, M.H. Ginsberg, I.A. Awad, and D.A. Marchuk. 2011. A novel mouse model of cerebral cavernous malformations based on the two-hit mutation hypothesis recapitulates the human disease. *Hum. Mol. Genet.* 20:211–222. http://dx.doi.org/10.1093/hmg/ddq433

McDonald, D.A., C. Shi, R. Shenkar, R.A. Stockton, F. Liu, M.H. Ginsberg, D.A. Marchuk, and I.A. Awad. 2012. Fasudil decreases lesion burden in a murine model of cerebral cavernous malformation disease. *Stroke.* 43:571–574. http://dx.doi.org/10.1161/STROKEAHA.111.625467

Mehta, D., and A.B. Malik. 2006. Signaling mechanisms regulating endothelial permeability. *Physiol. Rev.* 86:279–367. http://dx.doi.org/10.1152/physrev.00012.2005

Mettouchi, A. 2012. The role of extracellular matrix in vascular branching morphogenesis. *Cell Adhes. Migr.* 6:528–534. http://dx.doi.org/10.4161/cam.22862

Millon-Frémillon, A., D. Bouvard, A. Grichine, S. Manet-Dupé, M.R. Block, C. Albiges-Rizo, A. Millon-Frémillon, and S. Manet-Dupé. 2008. Cell adaptive response to extracellular matrix density is controlled by ICAP-1-dependent beta1-integrin affinity. *J. Cell Biol.* 180:427–441. http://dx.doi.org/10.1083/jcb.200707142

Pagenstecher, A., S. Stahl, U. Sure, and U. Felbor. 2009. A two-hit mechanism causes cerebral cavernous malformations: complete inactivation of CCM1, CCM2 or CCM3 in affected endothelial cells. *Hum. Mol. Genet.* 18:911–918.

Papusheva, E., and C.-P. Heisenberg. 2010. Spatial organization of adhesion: force-dependent regulation and function in tissue morphogenesis. *EMBO J.* 29:2753–2768. http://dx.doi.org/10.1038/emboj.2010.182

Parsons, J.T., A.R. Horwitz, and M.A. Schwartz. 2010. Cell adhesion: integrating cytoskeletal dynamics and cellular tension. *Nat. Rev. Mol. Cell Biol.* 11:633–643. http://dx.doi.org/10.1038/nrm2957

Provenzano, P.P., D.R. Inman, K.W. Eliceiri, S.M. Trier, and P.J. Keely. 2008. Contact guidance mediated three-dimensional cell migration is regulated by Rho/ROCK-dependent matrix reorganization. *Biophys. J.* 95:5374–5384. http://dx.doi.org/10.1529/biophysj.108.133116

Riant, F., F. Bergametti, X. Ayrignac, G. Boulday, and E. Tournier-Lasserve. 2010. Recent insights into cerebral cavernous malformations: the molecular genetics of CCM. *FEBS J.* 277:1070–1075. http://dx.doi.org/10.1111/j.1742-4658.2009.07535.x

Rybak, J.-N., C. Roesli, M. Kaspar, A. Villa, and D. Neri. 2007. The extra-domain A of fibronectin is a vascular marker of solid tumors and metastases. *Cancer Res.* 67:10948–10957. http://dx.doi.org/10.1158/0008-5472.CAN-07-1436

Schwarzbauer, J.E., and D.W. DeSimone. 2011. Fibronectins, their fibrillogenesis, and in vivo functions. *Cold Spring Harb. Perspect. Biol.* 3. http://dx.doi.org/10.1101/cshperspect.a005041

Singh, P., C. Carraher, and J.E. Schwarzbauer. 2010. Assembly of fibronectin extracellular matrix. *Annu. Rev. Cell Dev. Biol.* 26:397–419. http://dx.doi.org/10.1146/annurev-cellbio-100109-104020

Sottile, J., and D.C. Hocking. 2002. Fibronectin polymerization regulates the composition and stability of extracellular matrix fibrils and cell-matrix adhesions. *Mol. Biol. Cell.* 13:3546–3559. http://dx.doi.org/10.1091/mbc.E02-01-0048

Sottile, J., F. Shi, I. Rublyevska, H.Y. Chiang, J. Lust, and J. Chandler. 2007. Fibronectin-dependent collagen I deposition modulates the cell response to fibronectin. *Am. J. Physiol. Cell Physiol.* 293:C1934–C1946. http://dx.doi.org/10.1152/ajpcell.00130.2007

Stockton, R.A., R. Shenkar, I.A. Awad, and M.H. Ginsberg. 2010. Cerebral cavernous malformations proteins inhibit Rho kinase to stabilize vascular integrity. *J. Exp. Med.* 207:881–896. http://dx.doi.org/10.1084/jem.20091258

Stratman, A.N., K.M. Malotte, R.D. Mahan, M.J. Davis, and G.E. Davis. 2009. Pericyte recruitment during vasculogenic tube assembly stimulates endothelial basement membrane matrix formation. *Blood.* 114:5091–5101. http://dx.doi.org/10.1182/blood-2009-05-222364

Theodossiou, T.A., C. Thrasivoulou, C. Ekwobi, and D.L. Becker. 2006. Second harmonic generation confocal microscopy of collagen type I from rat tendon cryosections. *Biophys. J.* 91:4665–4677. http://dx.doi.org/10.1529/biophysj.106.093740

Tomasini-Johansson, B.R., N.R. Kaufman, M.G. Ensenberger, V. Ozeri, E. Hanski, and D.F. Mosher. 2001. A 49-residue peptide from adhesin F1 of Streptococcus pyogenes inhibits fibronectin matrix assembly. *J. Biol. Chem.* 276:23430–23439. http://dx.doi.org/10.1074/jbc.M103467200

Tseng, Q., I. Wang, A. Duchemin-Pelletier, A. Azioune, N. Carpi, J. Gao, O. Filhol, M. Piel, M. Théry, and M. Balland. 2011. A new micropatterning method of soft substrates reveals that different tumorigenic signals can promote or reduce cell contraction levels. *Lab Chip.* 11:2231–2240. http://dx.doi.org/10.1039/c0lc00641f

Tseng, Q., E. Duchemin-Pelletier, A. Deshiere, M. Balland, H. Guillou, O. Filhol, and M. Théry. 2012. Spatial organization of the extracellular matrix regulates cell-cell junction positioning. *Proc. Natl. Acad. Sci. USA.* 109:1506–1511. http://dx.doi.org/10.1073/pnas.1106377109

Van Obberghen-Schilling, E., R.P. Tucker, F. Saupe, I. Gasser, B. Cseh, and G. Orend. 2011. Fibronectin and tenascin-C: accomplices in vascular morphogenesis during development and tumor growth. *Int. J. Dev. Biol.* 55:511–525. http://dx.doi.org/10.1387/ijdb.103243eo

Velling, T., J. Risteli, K. Wennerberg, D.F. Mosher, and S. Johansson. 2002. Polymerization of type I and III collagens is dependent on fibronectin and enhanced by integrins alpha 11beta 1 and alpha 2beta 1. *J. Biol. Chem.* 277:37377–37381. http://dx.doi.org/10.1074/jbc.M206286200

Whitehead, K.J., N.W. Plummer, J.A. Adams, D.A. Marchuk, and D.Y. Li. 2004. Ccm1 is required for arterial morphogenesis: implications for the etiology of human cavernous malformations. *Development.* 131:1437–1448. http://dx.doi.org/10.1242/dev.01036

Whitehead, K.J., A.C. Chan, S. Navankasattusas, W. Koh, N.R. London, J. Ling, A.H. Mayo, S.G. Drakos, C.A. Jones, W. Zhu, et al. 2009. The cerebral cavernous malformation signaling pathway promotes vascular integrity via Rho GTPases. *Nat. Med.* 15:177–184. http://dx.doi.org/10.1038/nm.1911

Wong, J.H., I.A. Awad, and J.H. Kim. 2000. Ultrastructural pathological features of cerebrovascular malformations: a preliminary report. *Neurosurgery.* 46:1454–1459. http://dx.doi.org/10.1097/00006123-200006000-00027

Yadla, S., P.M. Jabbour, R. Shenkar, C. Shi, P.G. Campbell, and I.A. Awad. 2010. Cerebral cavernous malformations as a disease of vascular permeability: from bench to bedside with caution. *Neurosurg. Focus.* 29:E4. http://dx.doi.org/10.3171/2010.5.FOCUS10121

Zawistowski, J.S., I.G. Serebriiskii, M.F. Lee, E.A. Golemis, and D.A. Marchuk. 2002. KRIT1 association with the integrin-binding protein ICAP-1: a new direction in the elucidation of cerebral cavernous malformations (CCM1) pathogenesis. *Hum. Mol. Genet.* 11:389–396. http://dx.doi.org/10.1093/hmg/11.4.389

Zawistowski, J.S., L. Stalheim, M.T. Uhlik, A.N. Abell, B.B. Ancrile, G.L. Johnson, and D.A. Marchuk. 2005. CCM1 and CCM2 protein interactions in cell signaling: implications for cerebral cavernous malformations pathogenesis. *Hum. Mol. Genet.* 14:2521–2531. http://dx.doi.org/10.1093/hmg/ddi256

Zhang, J., R.E. Clatterbuck, D. Rigamonti, D.D. Chang, and H.C. Dietz. 2001. Interaction between krit1 and icap1alpha infers perturbation of integrin beta1-mediated angiogenesis in the pathogenesis of cerebral cavernous malformation. *Hum. Mol. Genet.* 10:2953–2960. http://dx.doi.org/10.1093/hmg/10.25.2953

Zhang, J., S. Basu, D. Rigamonti, H.C. Dietz, and R.E. Clatterbuck. 2008. Krit1 modulates beta 1 integrin-mediated endothelial cell proliferation. *Neurosurgery.* 63:571–578, discussion :578. http://dx.doi.org/10.1227/01.NEU.0000325255.30268.B0

Zhang, X.A., and M.E. Hemler. 1999. Interaction of the integrin beta1 cytoplasmic domain with ICAP-1 protein. *J. Biol. Chem.* 274:11–19. http://dx.doi.org/10.1074/jbc.274.1.11

Zhou, X., R.G. Rowe, N. Hiraoka, J.P. George, D. Wirtz, D.F. Mosher, I. Virtanen, M.A. Chernousov, and S.J. Weiss. 2008. Fibronectin fibrillogenesis regulates three-dimensional neovessel formation. *Genes Dev.* 22:1231–1243. http://dx.doi.org/10.1101/gad.1643308

Zovein, A.C., A. Luque, K.A. Turlo, J.J. Hofmann, K.M. Yee, M.S. Becker, R. Fassler, I. Mellman, T.F. Lane, and M.L. Iruela-Arispe. 2010. Beta1 integrin establishes endothelial cell polarity and arteriolar lumen formation via a Par3-dependent mechanism. *Dev. Cell.* 18:39–51. http://dx.doi.org/10.1016/j.devcel.2009.12.006